Published by Avanti Publishers

Journal of Advanced Thermal Science Research

ISSN (online): 2409-5826

Three-Dimensional MHD Casson Fluid Flow with Hall Current and Thermal Radiation: Coupled Heat and Mass Transfer over a Vertically Stretched Surface in a Chemically Reactive Medium

Issah Abubakari* and Ibrahim Y. Seini

Department of Mathematics, Faculty of Physical Sciences, University for Development Studies, Tamale, Ghana

ARTICLE INFO

Article Type: Research Article

Academic Editor: Umair Sultan

Keywords:
Hall current
Casson fluid
Thermal radiation
Stretching sheet flow
Magnetohydrodynamics (MHD)

Timeline:
Received: February 16, 2026
Accepted: April 17, 2026
Published: May 11, 2026

Citation: Abubakari I, Seini IY. Three-dimensional MHD casson fluid flow with hall current and thermal radiation: Coupled heat and mass transfer over a vertically stretched surface in a chemically reactive medium. J Adv Therm Sci Res. 2026; 13(1): 1-28.

DOI: https://doi.org/10.15377/2409-5826.2026.13.1

ABSTRACT

This work examines a three-dimensional magnetohydrodynamic (MHD) Casson fluid flow over a linearly stretched vertical surface under the combined effects of Hall current, thermal radiation, chemical reaction, buoyancy, and Ohmic dissipation. The governing boundary layer equations are reduced to a system of nonlinear ordinary differential equations using similarity transformations and solved numerically with the aid of the Runge–Kutta–Fehlberg method in Maple. Particular emphasis is placed on Hall current–induced cross-flow, which generates a secondary velocity component and alters shear stress characteristics. The results indicate that increasing the magnetic and Hall parameters enhances both streamwise and cross-flow skin-friction coefficients, while reducing heat and mass transfer rates. Radiation thickens the thermal boundary layer and suppresses heat transfer, whereas Casson parameter increases the fluid resistance and weakens the thermal and solutal transport. Chemical reaction significantly enhances the mass transfer due to steeper concentration gradients, with negligible impact on heat transfer. The study provides a unified three-dimensional analysis that captures the coupled influence of Hall-induced cross-flow, radiation, and chemical reaction on momentum, heat, and mass transport. The findings offer greater physical insights into multi-physics interactions relevant to engineering systems such as polymer processing, metallurgical cooling, and biomedical flows.

*Corresponding Author
Email: abubakariissah992@gmail.com
Tel: +(233) 248506319

1. Introduction

A subset of non-Newtonian fluids with a distinct yield stress is known as Casson fluids, and they are becoming increasingly important in food processing, biomedical engineering, and industrial applications [1]. The ability to model fluids that do not flow until a critical stress is exceeded makes Casson fluids vital in understanding processes involving paints, inks, chocolate, and polymer solutions [2]. In biomedical contexts, the theory of Casson fluids provides valuable insights into blood rheology, which informs the analysis of cardiovascular disorders. This is also important in the design of medical devices [3]. The Casson model was developed to describe the motion of complex fluids and is widely used to study the behavior of materials and physiological fluids, particularly those exhibiting both viscous and elastic characteristics such as blood. Casson [4] first introduced a foundational analysis and identified its unique properties relevant to various applications, particularly in the context of blood flow, highlighting the fluid's infinite viscosity at a zero shear rate and shear-thinning behavior at higher shear rates, Dhange *et al*. [5].

The investigation of heat and mass transfer on 3-D radiative MHD Casson fluid flow across a stretching porous sheet with chemical reaction was examined by Yanala *et al*. [6]. Alqahtani [7] explored how Newtonian heating affected non-Newtonian fluid's MHD flow while Seini *et al*. [8] examined the Casson fluid boundary layer flow with radiative heat transfer on an exponentially stretched porous surface. Aloliga *et al*. [9] investigated the hydromagnetic boundary layer flow of Casson fluid over a porous inclined magnetized surface with radiation and convective boundary conditions. Sulemana *et al*. [10] studied the flow of the hydrodynamic boundary layer of a chemically reactive fluid across an exponentially stretched vertical surface with a transverse magnetic field in an unsteady permeable medium. Arthur *et al*. [11] examined the presence of a magnetic field, the flow of Casson fluid over a vertically permeable surface with chemical reaction. The steady state hydrodynamic non-Newtonian nanofluid with a mobile microorganism influenced by energy activation was explored by Dharmaiah *et al*. [12] whilst Ali *et al*. [13] analyzed the presence of thermoelectric and radiation in a hydromagnetic Casson nanofluid flow across a stretched surface. In engineering processes and industries, transforming applications involving heat exchangers, nuclear power plants, thermal energy storage, and advanced drug delivery systems, Casson nonfluids and MHD are vital parameters.

Salem & Abd El-Aziz [14] examined the impact of chemical reactions and Hall currents on the hydromagnetic flow of a vertical stretched surface that generates heat internally. The impact of heat source and magnetic field on a thermally radiative hybrid nanofluid flow in a permeable medium has been investigated by Fatima & Hymavathi [15]. An investigation of MHD Casson fluid flow with heat and mass transfer across a permeable stretched sheet has been reported by Asogwa & Ibe [16]. Dey & Borah [17] analyzed the flow of Casson fluid with heat transfer and its dual solutions across a shrinking sheet. Saidulu & Lakshmi [18] investigated the presence of thermal radiation, viscous dissipation and heat source or sink of MHD Casson fluid flow with slip effects over exponentially porous stretching sheet. Numerical solution of Casson hybrid nanofluid heat transfer over a vertically stretched sheet with magnetic field effect was studied by Alkasasbeh [19]. Makkar *et al*. [20], numerically investigated the influence of radiation and chemical reaction-induced MHD convective free stream nanofluid flow across a stretching cylinder. Symbolic and numerical analysis for mathematical problem-solving with Maple was investigated by Sawlat *et al*. [21]. Seini [22] further examined the internal heat generation with chemical reaction in the presence of heat and mass transfer from a convectively heated vertical surface. The influence of magnetic field on radiative Casson fluid flow across an exponentially stretched surface has been explored by Talla [23] and extended by Abubakari and Seini [24] who analyzed the Casson fluid flow via porous medium on an exponentially stretched surface when a chemical reaction and transverse magnetic field are present. Leelavathi *et al*. [25] analyzed the stagnation point of MHD Casson fluid flow towards an inclined permeable surface. The effects on magnetized Casson nanofluid velocity slip over a stretched cylinder: duality and stability analysis was examined by Yashkun *et al*. [26]. Akaje [27] explored the Casson nanofluid with viscous dissipation and inclined magnetic field in stagnation point for heat flow and mass transfer. Matveenko & Kirsanov [28] studied the Rheology of structured liquids whilst Hazarika & Konch [29] investigated the variable viscosity effects and thermal conductivity on MHD free convective flow along a vertically porous plate with viscous dissipation. Mahabaleshwar *et al*. [30] examined the point of

stagnation Brinkman flow of a nanofluid with heat radiation on a stretched plate. Noor *et al*. [31] explored the MHD squeezed flow of sodium alginate-based Casson hybrid nanofluid with Soret and Dufour effects. Their findings support the regulation of heat transfer rate and fluid velocities in many manufacturing processes and industrial applications.

Effects of radiation on stagnation point flow of Casson nanofluid over a stretching cylinder was studied by Mahabaleshwar *et al*. [32]. Abbas *et al*. [33] analyzed the generalized Fourier's and Fick's laws, heat and mass transfer of non-Newtonian fluid flow caused by an exponentially stretching Riga surface. Mehmood *et al*. [34] studied the Ion-slip and Hall current, which are two methods of heat transport in viscoplastic flow through porous elastic sheets. A constant proportional Caputo model for fractional magnetohydrodynamic Casson fluid flow with thermal radiation and buoyancy effects has been explored by Abbas *et al*. [35]. Mahboobtosi *et al*. [36] Comprehensively analyzed the properties of heat transmission in the Casson fluid squeezing flow between circular plates. A numerical treatment of unsteady three-dimensional hydromagnetic flow of a Casson fluid with Hall and radiation effects [37]. Casson fluid flow across a stretching sheet with changing viscosity and sinusoidal boundary conditions: modeling and theoretical overview was examined by Islam *et al*. [38]. Nasir *et al*. [39]. Computationally analyzed the magnetized Casson fluid flow with Joule heating, adjacent to a porous medium, stratification, multiple slip and chemical reaction. A fully developed electrically conducting free convection Casson fluid flow formed by two infinite vertical parallel plates with thermal radiation, Hall current, and rotation effects was investigated [40] Alhadhrami *et al*. [41] examined the local thermal non-equilibrium effects on the flow and heat transfer of non-Newtonian Casson fluid numerically simulated in a porous media. Varatharaj *et al*. [42] studied Hall current and radiative effects in Casson nanofluid flow across a stretched surface with activation energy, analyzed using machine learning The peristaltic transport of a non-Newtonian fluid obeying a Casson model with heat and mass transfer inside a vertical circular cylinder was studied [43]. Reddy *et al*. [44] analyzed the radiative three-dimensional MHD nanofluid flow across an exponentially stretched sheet with numerous slip effects under double Cattaneo-Christov diffusion effects. However, these existing studies on Casson and Casson nanofluids flow reveal that heat and momentum transport are strongly influenced by coupled effects of thermal radiation, electromagnetic forces, non-Newtonian rheology and advanced diffusion mechanisms. These effects significantly modify velocity and temperature fields in stretching, porous, and confined geometries, highlighting the necessity of incorporating multi-physics and non-classical for realistic engineering and biomedical applications.

Unlike previous studies that often examines the flow of Casson fluids under isolated or partially coupled physical effects, the present work develops a comprehensive three-dimensional model that simultaneously incorporates Hall current–induced cross-flow, thermal radiation, chemical reaction, buoyancy forces, and Ohmic dissipation within a unified magnetohydrodynamic Casson fluid framework. A key novelty of this study lies in explicitly capturing the secondary (spanwise) velocity generated by Hall currents and quantifying its impact on cross-flow skin friction, which has received limited attention in the literature.

Furthermore, the study analyzed the coupled influence of electromagnetic forces, radiative heat transfer, and reactive mass transport on momentum, thermal, and concentration boundary layers over a linearly stretched vertical surface. This integrated multi-physics treatment provides new insights into the interaction mechanisms governing shear stress redistribution, boundary layer development, and transport rates, thereby extending existing models and offering a more realistic representation of complex industrial and biomedical flow systems.

2. Mathematical Analysis

The current study is investigating the magnetohydrodynamic (MHD) Casson fluid flow and its correlation with the linearly stretching vertical surface in the presence of transverse magnetic field, buoyancy and thermal radiation in a chemically reactive medium. In Fig. (**1**), we have depicted the physical configuration with the x-axis aligned to the stretching surface ($U_w = ax$), for which a is a non-negative real number. The y-axis is assumed to be normal to the surface, while the z-axis indicates the spanwise direction in which Hall currents yield a secondary velocity component. In this flow, there is decay of the momentum boundary layer from the stretching surface to

the free-stream condition and a reduction of the thermal boundary layer from the wall temperature (T_w) to ambient fluid temperature (T_∞) and a reduction of the concentration boundary layer from the wall concentration C_w, to ambient concentration C_∞. The primary forces driving the model are the Buoyancy forces (due to thermal and concentration gradients), the Lorentz forces (result from the applied magnetic field acting both along the flow and in the spanwise direction caused by Hall current effects). Such forces, in addition to viscous diffusion, thermal conduction, mass diffusion and chemical reaction, characterize the momentum, energy and concentration transport.

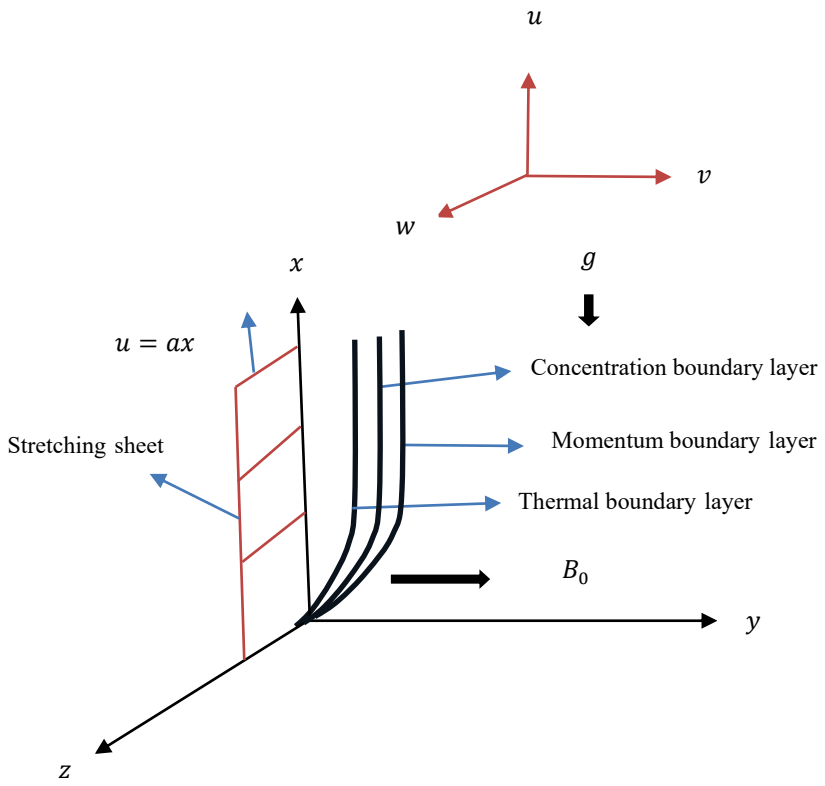

Figure 1: Physical diagram of the problem [13].

The rheological state equation for incompressible Casson fluid is given by [13, 18] as:

$$\tau = \begin{cases} 2\left(\mu_B + \frac{p_y}{\sqrt{2\pi}}\right) e_{ij}, & \pi > \pi_c \\ 2\left(\mu_B + \frac{p_y}{\sqrt{2\pi_c}}\right) e_{ij}, & \pi < \pi_c \end{cases} \tag{1}$$

In equation (1), $\pi\ equal\ e_{ij}e_{ij}$, where e_{ij} denotes the $(i,j)^{th}$ component of the deformation rate, π is the product of the component rate with itself, π_c is the critical value of this product based on the non-Newtonian model, μ_B is the plastic dynamic viscosity of the non-Newtonian fluid and P_y is the yield stress of the fluid [45].

The following equations characterize the physical conditions of the problem as in [13, 14, 46].

Continuity Equation

$$\frac{\partial u}{\partial x} + \frac{\partial v}{\partial y} = 0, \tag{2}$$

Momentum equation in (x and z) directions

$$u\frac{\partial u}{\partial x} + v\frac{\partial u}{\partial y} = \upsilon\left(1 + \frac{1}{\gamma}\right)\frac{\partial^2 u}{\partial y^2} - \frac{\sigma B_0^2}{\rho(1+m^2)}(u + mw) + g\beta_T(T - T_\infty) + g\beta_c(C - C_\infty), \tag{3}$$

$$u\frac{\partial w}{\partial x} + v\frac{\partial w}{\partial y} = v\left(1+\frac{1}{\gamma}\right)\frac{\partial^2 w}{\partial y^2} - \frac{\sigma B_0^2}{\rho(1+m^2)}(w-mu), \tag{4}$$

Energy Equation

$$u\frac{\partial T}{\partial x} + v\frac{\partial T}{\partial y} = \alpha\frac{\partial^2 T}{\partial y^2} - \frac{1}{\rho c_p}\frac{\partial qr}{\partial y} + \frac{\sigma B_0^2}{\rho(1+m^2)}(u^2+w^2), \tag{5}$$

Concentration Equation

$$u\frac{\partial C}{\partial x} + v\frac{\partial C}{\partial y} = D\frac{\partial^2 C}{\partial y^2} - k_1(C-C_\infty), \tag{6}$$

Boundary conditions are

$$\begin{aligned} &u = U_w = ax, v = w = 0, C = C_w, T = T_{w,} \; at \; y = 0, \\ &u = v = w = 0, \; T \to T_\infty, C \to C_\infty, as \; y \to \infty, \end{aligned} \tag{7}$$

where, w is the secondary velocity component obtained by using the Hall current, u and v represent the main velocity components in the x x and y axes, respectively, ρ is the fluid density, β is the exchange of heat and mass expansion coefficient, m is the Hall current parameter, and v is the kinematic viscosity, g is the acceleration due to gravity, c_p is specific heat capacity at constant pressure, B_0 indicates the magnetic induction field, and the electrical conductivity is represented by σ, α is the fluid thermal diffusivity, D is the mass diffusivity, k_1 indicates the reaction rate and γ represents the Casson parameter.

In modeling the thermal radiation, the fluid is assumed to be optically thick and gray, which permits the use of the Rosseland diffusion approximation. In the Rosseland approximation, the radiative heat flux is taken as $q_r = -\frac{4}{3}\frac{\sigma^*}{k^*}\frac{\partial T^4}{\partial y}$ where k* is the absorption parameter and σ* indicates the Stefan-Boltzmann constant. Assuming a relatively small temperature differential, we adopt the expression $T^4 \approx 4T_\infty^3 T - 3T_\infty^4$ and express T^4 by Taylor's estimate at T_∞ (Ignoring higher-order terms) [47, 48].

The following similarity variables are introduced to transform the governing partial differential equations into a set of coupled ordinary differential equations [49, 50]:

$$\begin{aligned} &\eta = y\sqrt{\frac{a}{v}}, \qquad \psi = \sqrt{av}\, x\, f(\eta), \qquad u = axf'(\eta), \qquad v = -\sqrt{av}\, f(\eta), \qquad w = axg(\eta), \\ &\theta(\eta) = \frac{T-T_\infty}{T_w - T_\infty}, \; \phi(\eta) = \frac{C-C_\infty}{C_w - C_\infty} \end{aligned} \tag{8}$$

Equations (2) – (6) are transformed using (8) to:

$$\left(1+\frac{1}{\gamma}\right)f''' + ff'' - f'^2 - M(f'+mg) + Gr\theta + Gm\emptyset = 0, \tag{9}$$

$$\left(1+\frac{1}{\gamma}\right)g'' - M(g-mf') - f'g + fg' = 0, \tag{10}$$

$$\left(1+\frac{4}{3}Nr\right)\theta'' + Prf\theta' + MPrEc\left(f'^2 + g'^2\right) = 0, \tag{11}$$

$$\emptyset'' + Scf\emptyset' - \lambda Sc\emptyset = 0. \tag{12}$$

With the associated dimensionless boundary conditions;

$$\begin{aligned} &f(0) = 0, f'(0) = 1, g(0) = 0, \theta(0) = 1, \emptyset(0) = 1, \\ &f'(\infty) = 0, g(\infty) = 0, \emptyset(\infty) = 0, \theta(\infty) = 0, \end{aligned} \tag{13}$$

where $M,\ Pr, m,\ Sc, Ec,\ Gr,\ Gm,\ Nr, \lambda,\ C_f, Nu, Sh,\ Re_x$ are the parameters and numbers used, including magnetic parameter, Prandtl number, Hall current effect, Eckert number, Schmidt number, Thermal Grashof number, Solutal Grashof number, radiation parameter, reaction rate parameter, skin-friction coefficients, Nusselt number, Sherwood number, and Reynolds number, respectively expressed as in equation (14).

$$M = \frac{\sigma B_0^2}{\rho a(1+m^2)}, Pr = \frac{\nu}{\alpha}, \qquad Sc = \frac{\nu}{D}, \qquad Ec = \frac{U_w^2}{c_p(T_w - T_\infty)}, \qquad Gr = \frac{g\beta_T(T_w - T_\infty)}{a^2 x},$$

$$Gm = \frac{g\beta_c(C_w - C_\infty)}{a^2 x},\ Nr = \frac{16\sigma^* T_\infty^3}{3k^* k},\ \lambda = \frac{k_1}{a} \tag{14}$$

The most important quantities of practical relevance to engineers are the local skin friction coefficients, the rate of heat transfer (the Nusselt number), and the rate of mass transfer (the Sherwood number) obtained in equation (15).

$$\left(1+\frac{1}{\gamma}\right) f''(0) = C_f\sqrt{Re_x},\ \left(1+\frac{1}{\gamma}\right) g'(0) = C_f\sqrt{Re_x}, -\theta'(0) = \frac{Nu_x}{\sqrt{Re_x}}, -\emptyset'(0) = \frac{Sh_x}{\sqrt{Re_x}}, \tag{15}$$

3. Method of Solution

Equations (9) – (12) are higher-order non-linear ordinary differential equations. Obtaining an exact solution to this set of equations is very difficult. Therefore, the equations are reduced to coupled first-order ordinary differential equations solved using the fourth-fifth order Runge-Kutta Fehlberg method. Graphical and numerical data are obtained in Maple 22 software for the velocity, temperature and concentration profiles and discussed quantitatively.

In the process, we let:

$y_1 = f,\ y_2 = f',\ y_3 = f'',\ y_4 = g,\ y_5 = g',\ y_6 = \theta,\ y_7 = \theta',\ y_8 = \emptyset,\ y_9 = \emptyset'$,

Therefore:

$y_1' = y_2,$

$y_2' = y_3,$

$y_3' = \frac{y_2^2 + M(y_2 + my_4) - y_1 y_3 - Gry_6 - Gmy_8}{1+\frac{1}{\gamma}},$

$y_4' = y_5,$

$y_5' = \frac{M(y_4 - my_2) + y_2 y_4 - y_1 y_5}{1+\frac{1}{\gamma}},$ (16)

$y_6' = y_7,$

$y_7' = \frac{-Pry_1 y_7 - MPrEc(y_2^2 + y_5^2)}{1+\frac{4}{3}Nr},$

$y_8' = y_9,$

$y_9' = -Scy_1 y_9 + \lambda \mathrm{Sc} y_8.$

If we let $y = (y_1, \ldots, y_9)$,

Then,

$$y' = \begin{bmatrix} y_2 \\ y_3 \\ \frac{y_2^2 + M(y_2 + my_4) - y_1 y_3 - Gry_6 - Gmy_8}{1+\frac{1}{\gamma}} \\ y_5 \\ \frac{M(y_4 - my_2) + y_2 y_4 - y_1 y_5}{1+\frac{1}{\gamma}} \\ y_7 \\ \frac{-Pry_1 y_7 - MPrEc(y_2^2 + y_5^2)}{1+\frac{4}{3}Nr} \\ y_9 \\ -Scy_1 y_9 + \lambda Scy_8 \end{bmatrix} \quad (17)$$

If $y_3 = f"(0) = a, y_5 = g'(0) = b,\ y_7 = \theta'(0) = c$ and $y_9 = \emptyset(0) = d$

Then the initials conditions are:

$$\begin{pmatrix} y_1 \\ y_2 \\ y_3 \\ y_4 \\ y_5 \\ y_6 \\ y_7 \\ y_8 \\ y_9 \end{pmatrix} = \begin{pmatrix} 0 \\ 1 \\ a \\ 0 \\ b \\ 1 \\ c \\ 1 \\ d \end{pmatrix} \quad (18)$$

The method is preferred because of its consistency, and the ability to handle nonlinear ordinary differential equations efficiently has made it a great topic of interest in research. Particularly, it executes with a step size of $\eta = 0.01$ near the wall where the solutions change quickly. The problem is resolved with an interval ranging $0 \leq \eta \leq 10$, with $\eta \to \infty$. The criteria of convergence is 10^{-5}. A trial-and-error approach was used to arrive at this. The procedure is also shown in the flow chart (Fig. **2**).

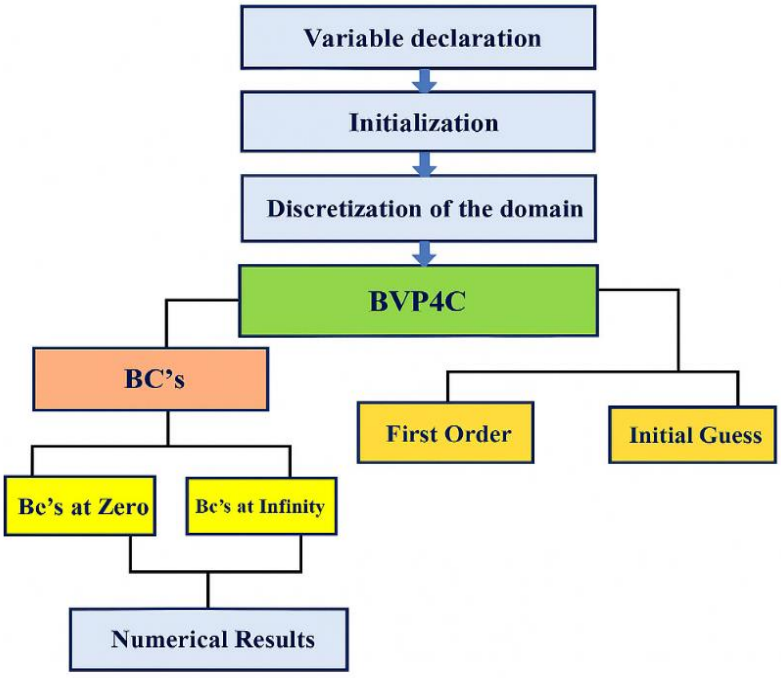

Figure 2: Process flow diagram for calculating results [12].

4. Comparison of Present Numerical Results

From Table **1**, it is evident that the skin friction co-efficient and the rate of mass transfer perfectly agree with results in [11] for M, γ, Gm, Sc, λ, with $Ec = Nr = Pr = Gr = 0$ as $f_w = 0.1$. This numerical result shows the robustness of the proposed scheme.

Table 1: Comparison of results for $f''(0)$, and $-\emptyset'(0)$ with [11].

M	γ	Gm	Sc	λ	f_w	Ref. [11]		Present	
						$-f''(0)$	$-\emptyset'(0)$	$-f''(0)$	$-\emptyset'(0)$
0.5	0.5	0.1	0.6	0.3	0.1	0.701894	0.675765	0.701894	0.675765
0.7						0.747866	0.670528	0.747866	0.670528
1.0						0.812075	0.663476	0.812075	0.663476

Table 2: Comparison of results for the rate of heat transfer with [51].

Pr	Ref. [51]	Present
	$-\theta'(0)$	$-\theta'(0)$
0.001	0.017316	0.01784
0.01	0.051589	0.05643
0.1	0.140034	0.17847
1	0.33206	0.33206
10	0.728141	0.72814

Table **2** shows the values of the Nusselt number ($-\theta'(0)$) in Newtonian fluid when the rest of the parameters $= 0$.

5. Results and Discussions

Table **3** presents the computed values of the skin-friction coefficients $(-f''(0), -g'(0))$, the local Nusselt number $(-\theta'(0))$, and the local Sherwood number $(-\phi'(0))$for various combinations of governing parameters. The baseline case is $Pr = 0.7$, $\gamma = 1$, $M = 1$, $m = 0.5$, $Ec = 0.01$, $Gr = 0.2$, $Gm = 0.1$, $Nr = 0.5$, $\lambda = 0.001$, $Sc = 0.6$, which yields:

$$(-f''(0), -g'(0), -\theta'(0), -\phi'(0)) = (0.90530,\ 0.14692,\ 0.36213,\ 0.43065).$$

It is clearly observed that as the Prandtl number increases, it markedly enhances the heat transfer rate. This occurs as a result of a higher Prandtl number, which reduces thermal diffusivity, thereby thinning the thermal boundary layer. The skin-friction coefficient and Sherwood number exhibit minor changes, confirming that Prandtl numbers predominantly affect thermal transport. As the Casson parameters increase, the streamwise skin-friction rises, as well as the cross-flow shear. These increases deflect the enhanced resistance of Casson fluids to deformation. Conversely, both the heat transfer and the mass transfer rates decrease, indicating that stronger yield stress thickens the thermal and the concentration boundary layers. The raising of the Hall current parameter substantially augments wall shear, leading to an increase in both the skin-friction coefficient in the x-direction and the z-direction.

Meanwhile, the heat and mass transfer rates decrease monotonically. Thus, Hall current enhances electromagnetic resistance, reinforcing the shear stress but weakening the heat and mass transfer at the surface. With a stronger magnetic field, both shear coefficients increase, particularly in the cross-flow direction. However, the Nusselt and Sherwood numbers decrease.

Table 3: Numerical values for the skin friction coefficients, local Nusselt number and the local Sherwood number under various thermophysical conditions.

Pr	γ	M	m	Ec	Gr	Gm	Nr	λ	Sc	$-f''(0)$	$-g'(0)$	$-\theta'(0)$	$-\emptyset'(0)$
0.71	1	1	0.5	0.01	0.2	0.1	0.5	0.001	0.6	0.90530	0.14692	0.36213	0.43065
5.0										0.93993	0.14087	1.23885	0.41611
7.1										0.94475	0.14048	1.51337	0.41513
0.7	2									1.03643	0.17219	0.34509	0.41133
	3									1.09562	0.18377	0.33835	0.40353
	4									1.12953	0.19045	0.33472	0.39931
	1	2								1.15103	0.22680	0.32276	0.38841
		3								1.35680	0.28580	0.29466	0.35716
		4								1.53682	0.33438	0.27358	0.33312
		1	1.0							0.93487	0.28425	0.35129	0.41911
			1.5							0.97648	0.40739	0.33649	0.40307
			2.0							1.02419	0.51647	0.32043	0.38516
			0.5	1						0.89894	0.14798	0.12699	0.43310
				2						0.89223	0.14909	0.11624	0.43565
				3						0.88523	0.15025	0.36580	0.43830
				0.01	0.4					0.83787	0.15333	0.37578	0.44541
					0.6					0.77268	0.15900	0.38749	0.45809
					0.8					0.70931	0.16414	0.39781	0.46929
					0.2	0.3				0.84207	0.15231	0.37366	0.44326
						0.5				0.78072	0.15717	0.38378	0.45434
						0.7				0.72095	0.16161	0.39285	0.46428
						0.1	1.0			0.90046	0.14832	0.29963	0.43367
							1.5			0.89713	0.14937	0.26022	0.43584
							2.0			0.89472	0.15016	0.23329	0.43733
							0.5	0.4		0.90990	0.14604	0.36017	0.66596
								0.6		0.91129	0.14581	0.35965	0.75442
								0.8		0.91242	0.14563	0.35926	0.83285
								0.001	0.8	0.90801	0.14632	0.36078	0.52236
									1.0	0.91011	0.14591	0.35988	0.60457
									1.2	0.91179	0.14562	0.35923	0.67951

This reflects the Lorentz force damping of velocity coupled with joule heating, which suppresses thermal and solutal gradients. An increase in the solutal Grashof number leads to a rise in mass transfer rate, corresponding to an increase of about 5%. However, the concentration profiles appear thicker for a larger solutal Grashof number. The critical factor is the wall slope, which becomes steeper, thereby enhancing solutal transfer. As the Eckert number increases, the streamwise skin-friction coefficient decreases slightly due to joule heating reducing near-wall velocity gradients, while the cross-flow shear rises modestly. The Nusselt number initially falls, confirming that ohmic dissipation thickens the thermal boundary layer and weakens wall heat transfer. However, the variation of

the Nusselt number with the Eckert number exhibits a non-monotonic behavior. Initially, as Ec increases, the Nusselt number decreases due to enhanced viscous and Ohmic dissipation, which thickens the thermal boundary layer and reduces the wall temperature gradient. However, beyond a certain threshold, a further increase in Ec leads to a significant rise in the Nusselt number. This indicates that at higher dissipation levels, internal heat generation intensifies the near-wall temperature gradient, thereby enhancing heat transfer. This transition reflects a shift from diffusion-dominated to dissipation-dominated thermal transport. By contrast, the Sherwood number increases monotonically, indicating that stronger joule heating intensifies solutal diffusion via thermo-solutal coupling. Increasing thermal buoyancy strengthens mixed/free convection. It relieves viscous burden in the streamwise layer (skin-friction) while enhancing both heat and mass transfer. Solutal buoyancy acts analogously to thermal buoyancy. As solutal Grashof grows, solutal free convection strengthens, reducing streamwise wall shear and boosting both heat and especially mass transfer.

Increasing the radiation parameter (N_r) produces contrasting effects on wall transport characteristics. Streamwise skin friction decreases slightly as radiative heating reduces velocity gradients, while cross-flow shear rises modestly due to enhanced secondary flow. The Nusselt number decreases markedly, indicating that stronger radiation thickens the thermal boundary layer and weakens wall heat transfer. Conversely, the Sherwood number increases slightly, showing that radiation enhances the solutal concentration gradient at the wall and promotes mass transfer. Increasing the reaction parameter (λ) markedly enhances mass transfer while leaving heat transfer and wall shear almost unchanged. Numerically, the Sherwood number rises to (≈25%), reflecting a steeper wall concentration gradient produced by stronger near-wall consumption of species. The Nusselt number varies by less than 0.3%, confirming that the reaction primarily alters the solutal field with minimal thermal impact. Skin-friction coefficients change only marginally (streamwise slightly higher, cross-flow slightly lower), indicating weak momentum sensitivity to reaction rate. Increasing the Schmidt number substantially enhances wall mass transfer, with the Sherwood number rising by ≈16% to 30% respectively. This reflects the reduction in species diffusivity at higher Sc, which compresses the concentration boundary layer and steepens the wall concentration gradient. In contrast, the thermal field is only weakly affected as the Nusselt number decreases by less than 0.5% across the sweep, indicating essentially unchanged wall heat transfer. The momentum response is minimal, with a slight increase in streamwise skin friction and a slight decrease in cross-flow skin friction.

The cross-flow skin-friction coefficient is strongly influenced by electromagnetic and transport parameters, particularly the magnetic parameter M, Hall parameter m, radiation parameter N_r, and chemical reaction parameter λ. An increase in M enhances the Lorentz force, which suppresses the primary flow and redirects momentum into the transverse direction, thereby increasing cross-flow shear at the wall. Similarly, increasing the Hall parameter m intensifies the cross-flow motion by promoting current deflection, leading to a significant rise in the cross-flow skin-friction coefficient. In contrast, higher radiation parameter N_r slightly elevates cross-flow shear due to thermal softening of the fluid, which reduces effective viscosity and facilitates transverse motion. The chemical reaction parameter λ however, has only a marginal effect on cross-flow skin friction, indicating weak coupling between reactive mass transfer and momentum transport in the spanwise direction. These findings are of practical importance in systems such as MHD pumps, polymer extrusion, and plasma devices, where enhanced cross-flow shear can improve mixing and surface transport but may also increase mechanical stress on the stretching surface.

Fig. (**3**) illustrates that increasing the magnetic parameter Msuppresses fluid motion due to the Lorentz force, leading to thinner boundary layers, while Casson fluids retain higher velocities compared to Newtonian fluids. Physically, the Lorentz force generated by the applied magnetic field suppresses fluid motion. For cross-flow velocity in (Fig. **4**), increasing the magnetic parameter amplifies the flow and brings its peak closer to the wall, after which it decays more quickly. Physically, the magnetic field dampens the streamwise motion but diverts momentum into the Hall direction, intensifying the secondary flow near the wall while localizing it within a thinner layer. Casson fluid behavior tends to thicken the momentum layer and suppress cross-flow relative to Newtonian flow. Practice in liquid metal casting and plasma control, higher magnetic fields suppress velocity but intensify cross-flow shear.

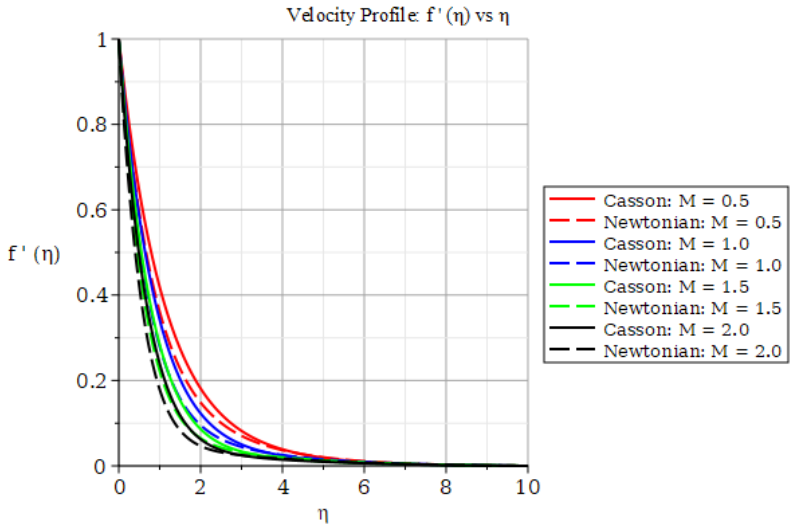

Figure 3: Varying the magnetic parameter for the Primary velocity.

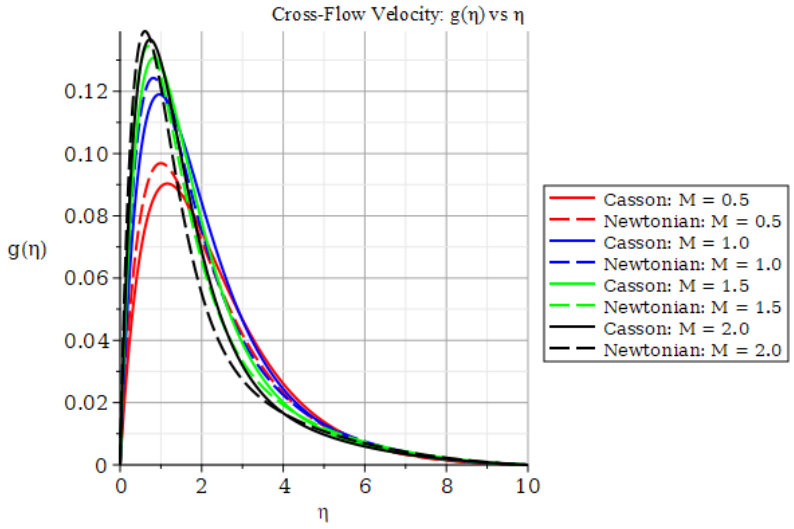

Figure 4: Significant impact of the Magnetic parameter on the Secondary velocity.

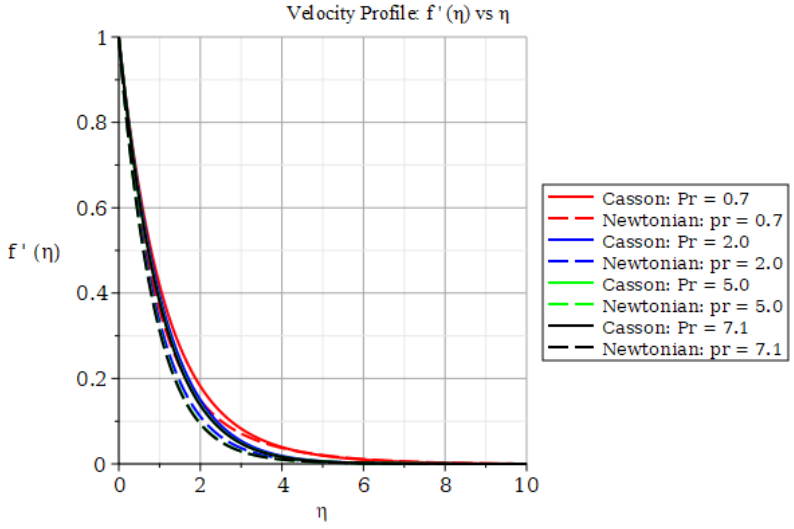

Figure 5: Vital impact of Prandtl number on primary velocity.

The streamwise velocity (Fig. **5**) demonstrates that increasing the Prandtl number accelerates the decay of velocity, resulting in thinner momentum boundary layers and higher wall shear stresses. Conversely, the cross-flow velocity profiles g(η) reveal that higher Pr suppresses the Hall-induced secondary motion, lowering the peak magnitude and confining it nearer to the wall (Fig. **6**). Newtonian fluids consistently show faster velocity decay and stronger cross-flow peaks compared to Casson fluids, indicating higher skin-friction coefficients in both directions. These results confirm that the Prandtl number exerts a dual role, strengthening streamwise shear while diminishing cross-flow transport.

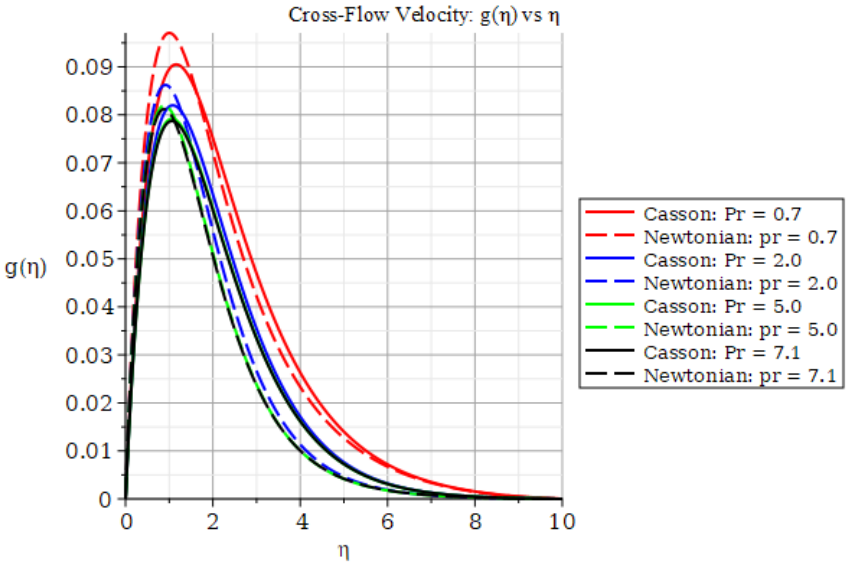

Figure 6: Significant impact of Prandtl number on Secondary velocity.

As can be seen in Fig. (**7**), the Casson parameter is inversely related to the yield stress. A small Casson value makes it resist fluid deformation strongly as the velocity persists farther from the wall, thickening the momentum boundary layer and lowering the wall shear. Fig. (**8**) depicts the cross-flow velocity as the Casson parameter grows, the effective viscosity decreases, allowing the cross-flow velocity to intensify and peak earlier. These results confirm that Casson rheology moderates momentum and cross-flow transport, while the Newtonian limit exhibits the strongest shear stresses. Blood and industrial yield-stress fluids illustrate how non-Newtonian behavior reduces shear, producing thicker velocity layers than Newtonian flows.

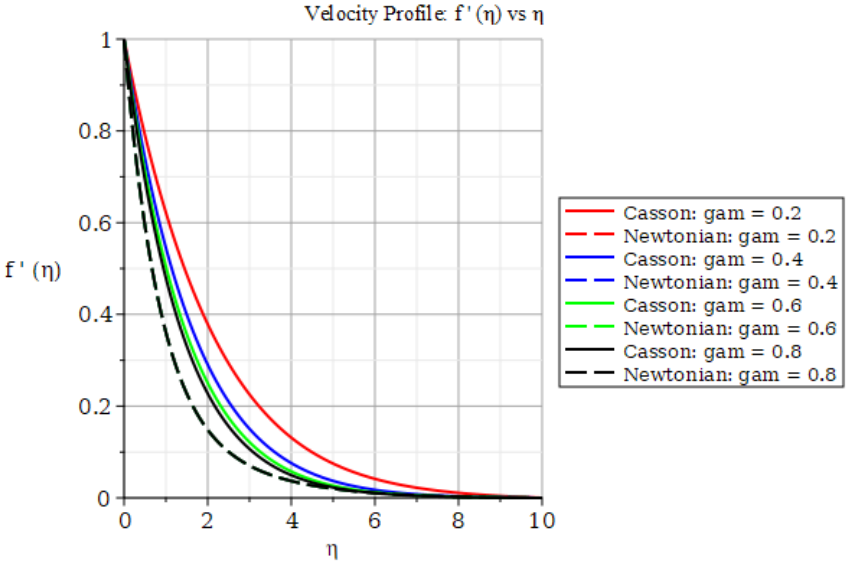

Figure 7: Vital impact of the Casson parameter on the primary velocity.

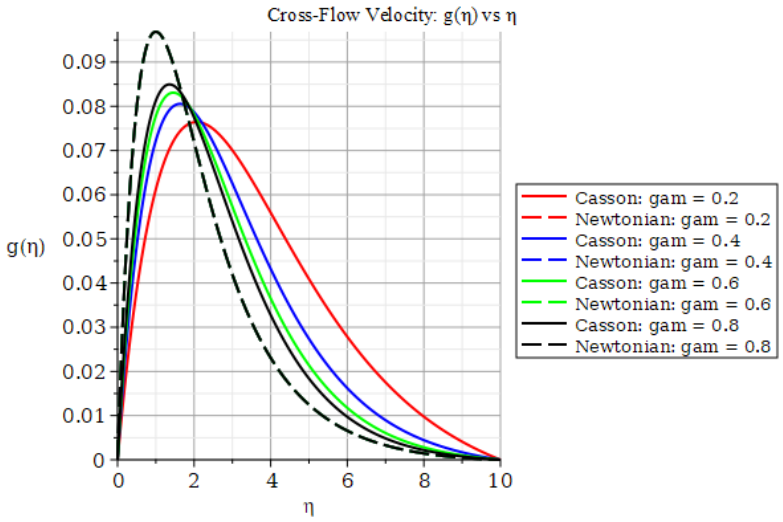

Figure 8: Significant impact of the Casson parameter on the secondary velocity.

Fig. (**9**) presents the impact of the Hall current on the velocity profile, indicating that the velocity falls as the Hall current effect increases. Larger Hall current allows stronger cross-field motion, which reduces the effective resistance along the streamwise direction, thus momentum diffuses faster, which leads to thinning of the boundary layer. Simultaneously, the Hall-induced cross-flow velocity is intensified, which peaks higher and closer to the wall, raising the cross-flow skin friction coefficient (Fig. **10**). Casson fluids exhibit thicker boundary layers and weaker cross-flows compared to Newtonian fluids at the same Hall current effect, confirming that yield-stress effects moderate the influence of Hall currents on both primary and secondary velocity fields. Hall thrusters and ionospheric plasmas exemplify how stronger Hall effects enhance cross-flow motion and wall shear while weakening convective transport.

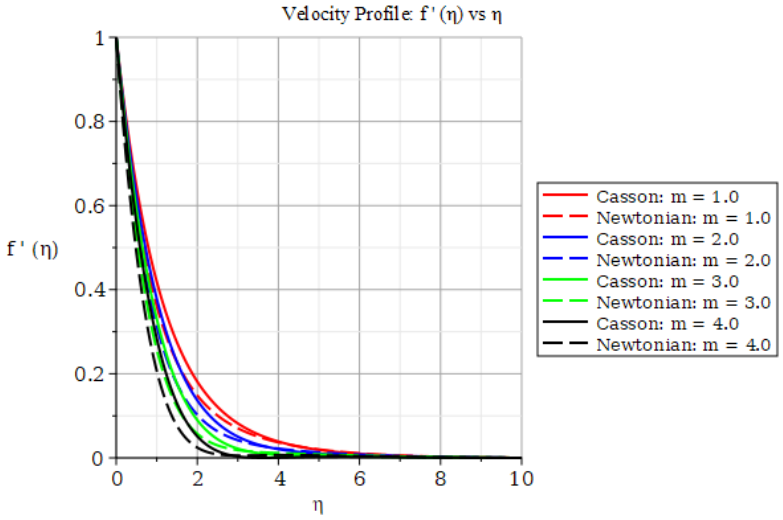

Figure 9: Essential impact of Hall current effect on the primary velocity.

The thermal Grashof number Gr plays a critical role in buoyancy-driven convection. As Gr increases, buoyancy forces accelerate the streamwise velocity, thickening the momentum boundary layer (Fig. **11**). While simultaneously enhancing the Hall-induced cross-flow velocity, which rises to higher peaks nearer the wall (Fig. **12**). Newtonian fluids display sharper velocity decay and stronger cross-flows than Casson fluids, whereas Casson rheology moderates both streamwise and cross-flow accelerations due to its yield-stress effects. These results confirm that thermal buoyancy promotes both primary and secondary velocity fields, with Newtonian fluids responding more strongly than Casson fluids.

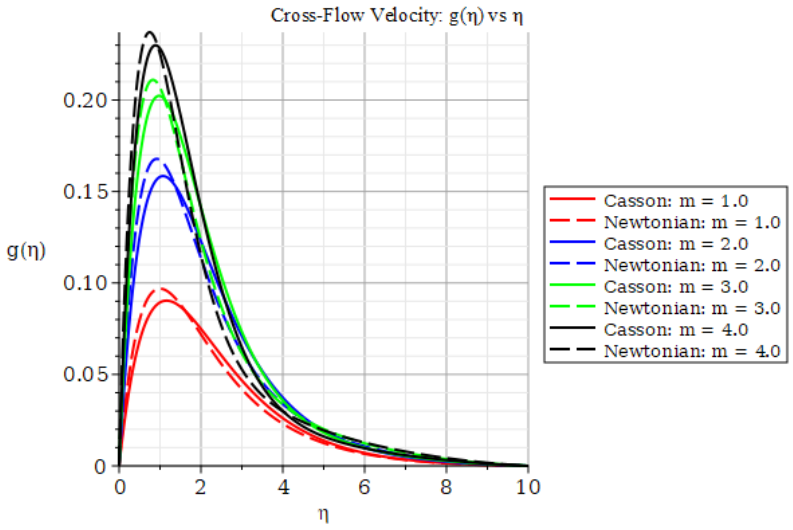

Figure 10: Vital impact of the Hall current effect on the secondary velocity.

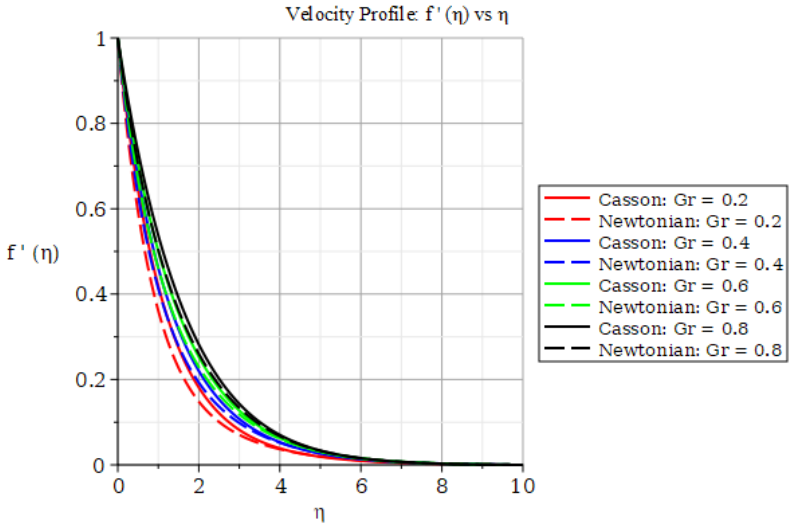

Figure 11: Vital impact of thermal Grashof number on the velocity.

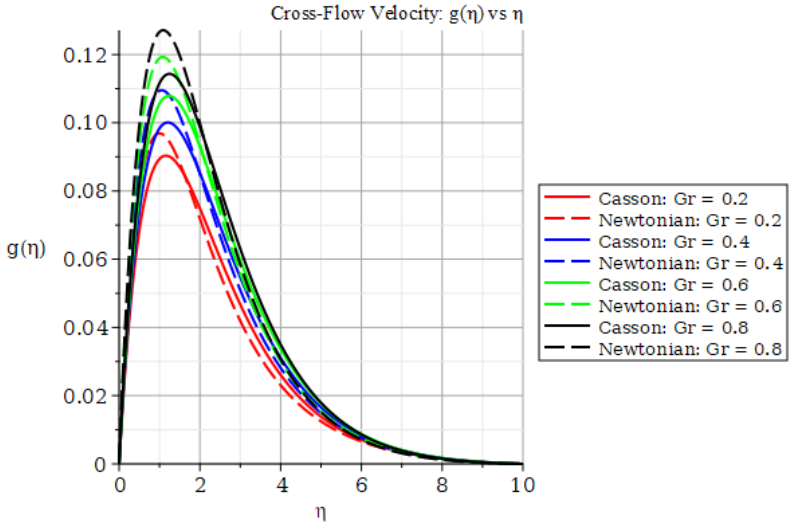

Figure 12: Significant impact of thermal Grashof number on the velocity.

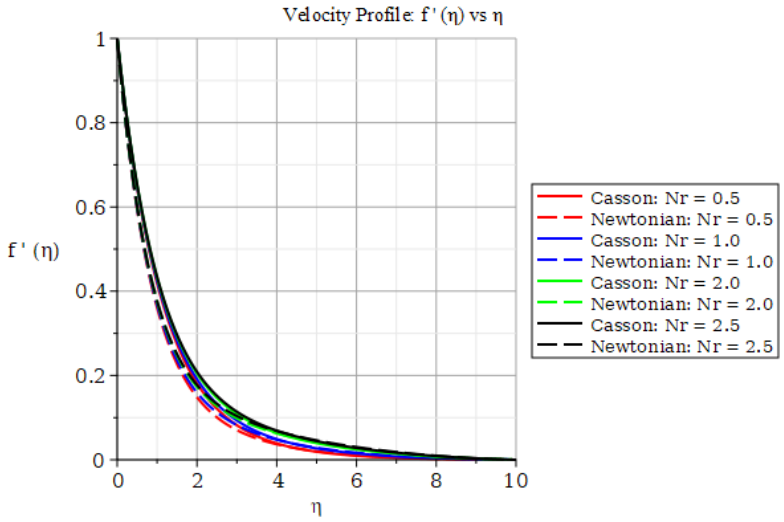

Figure 13: The vital impact of the radiation parameter on the velocity.

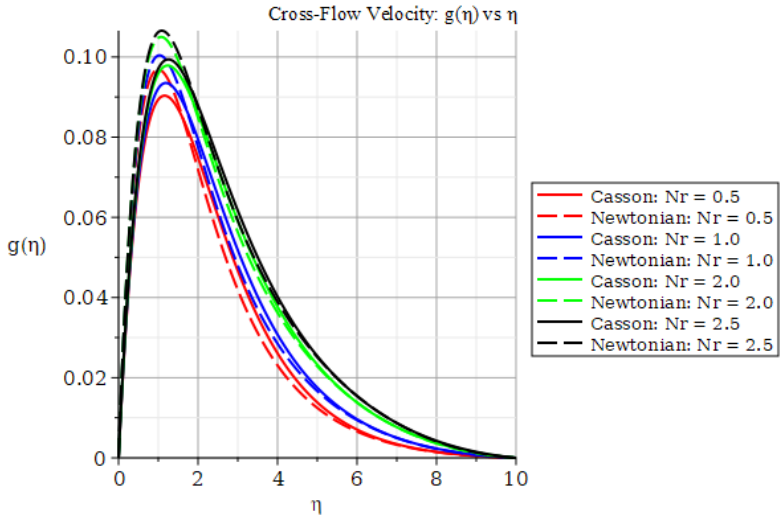

Figure 14: Vital impact of radiation parameter on the secondary velocity profile.

The radiation parameter enhances radiative heat transfer, which warms the near-wall fluid and reduces momentum loss. Therefore, higher radiation effectively dampens the retarding magnetic or viscous forces, allowing velocity to persist further from the wall. Physically, it acts as a volumetric heating mechanism, thickening the thermal boundary layer and weakening convective cooling at the surface (Fig. **13**). Consequently, radiation raises the fluid temperature, thereby reducing viscous resistance and allowing more momentum to be diverted into the Hall-induced secondary motion (Fig. **14**). Casson fluids display weaker cross-flow velocities and thicker boundary layers compared to Newtonian fluids, reflecting the moderating role of yield-stress rheology. These results confirm that radiation enhances both thermal and momentum transport, but with contrasting effects on streamwise and cross-flow shear.

It is interesting to note that the combined influence of the Hall parameter m and radiation parameter N_r acts to thin the momentum boundary layer and enhance cross-flow velocities. As m rises from 0.5 to 2.0, with N_r Simultaneously increasing from 0.5 to 2.0, the streamwise velocity decays more rapidly, reflecting higher wall shear stresses (Fig. **15**). Concurrently, the Hall-induced cross-flow velocity becomes significantly stronger, with peaks moving closer to the wall and attaining larger magnitudes (Fig. **16**). Newtonian fluids consistently exhibit sharper gradients and stronger cross-flows than Casson fluids, highlighting that yield-stress effects moderate the combined magnetic thermal interactions in the flow.

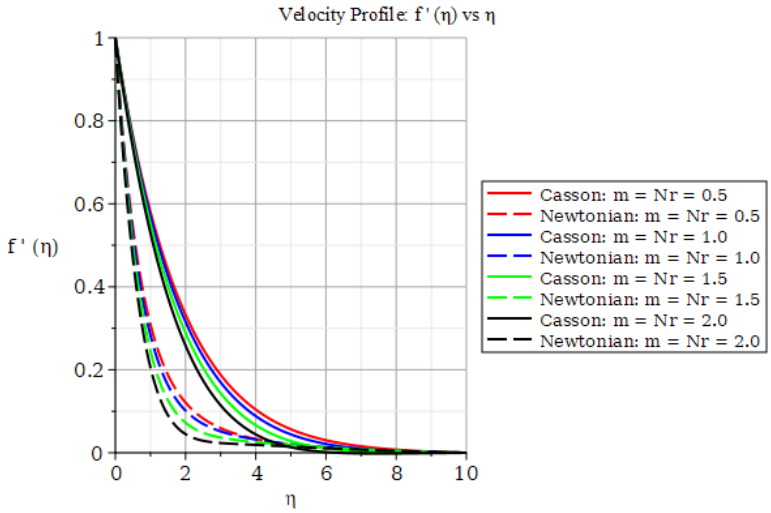

Figure 15: Essential impact of Hall current effect and radiation on the velocity.

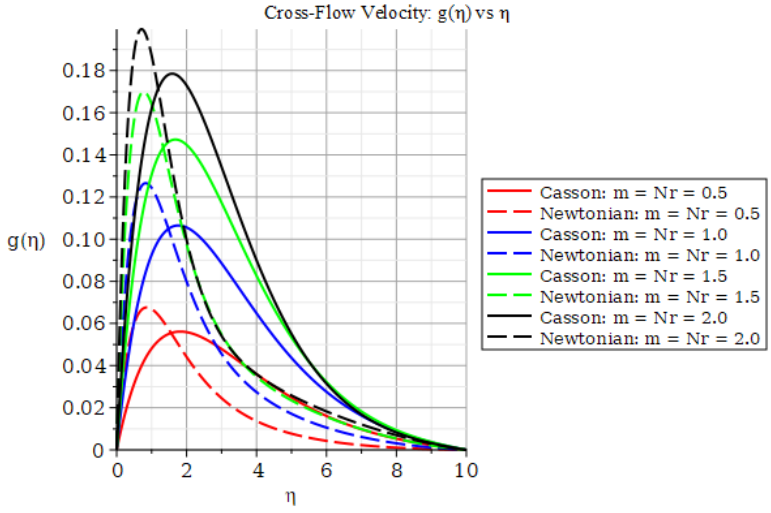

Figure 16: Significant impact of the Hall current effect and the radiation on velocity.

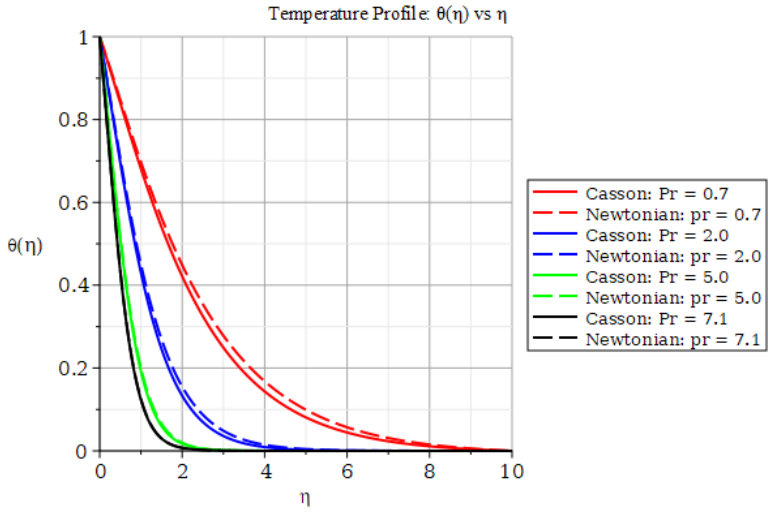

Figure 17: Significant impact of Prandtl number on temperature.

Fig. (**17**) clearly demonstrates the influence of the Prandtl number (Pr). As Pr increases from 0.7 to 7.1, the thermal boundary layer becomes progressively thinner with the temperature decaying more sharply away from the wall. This occurs because high Pr fluids (such as oils) possess low thermal diffusivity, restricting heat conduction to a narrow region near the wall, while low Pr fluids (such as air) allow heat to diffuse deeper into the fluid. Newtonian fluids exhibit slightly thinner thermal layers than Casson fluids due to the absence of yield-stress effects. The steeper wall gradients at higher Pr correspond directly to an increase in the Nusselt number, confirming that heat transfer at the wall is strongly enhanced in high Pr fluids.

The Magnetic parameter M increases the Lorentz force, which suppresses fluid motion and convective cooling. As M rises, the temperature profile decays more slowly, the thermal boundary layer thickens, and the wall temperature gradient decreases. This leads to a reduction in the Nusselt number and hence a lower heat transfer rate, confirming that strong magnetic fields inhibit convective heat transport (Fig. **18**). Fig. (**19**) depicts the Casson parameter γ, which characterizes yield-stress effects, shows the opposite trend. Fluids with small γ(strong Casson effects) display thinner thermal boundary layers and larger wall gradients, corresponding to higher heat transfer rates. As γ increases toward the Newtonian limit, the boundary layer thickens, thermal decay slows, and the Nusselt number decreases. This indicates that Casson fluids, due to yield-stress resistance, enhance wall heat transfer relative to Newtonian fluids.

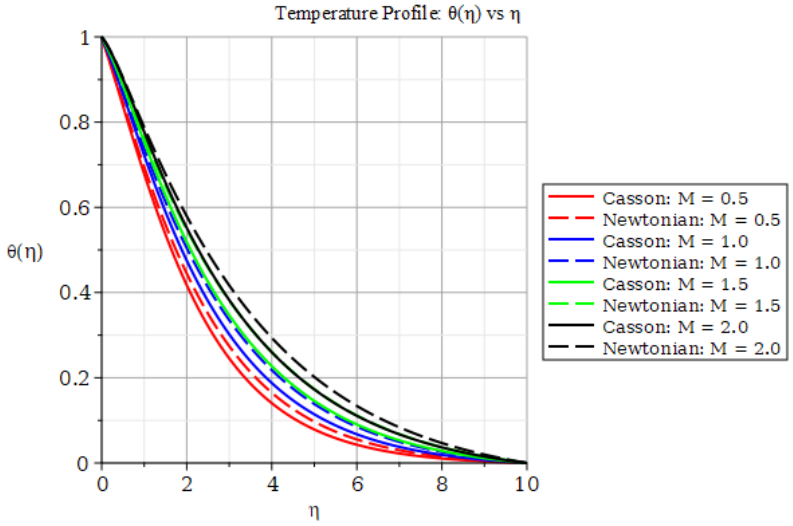

Figure 18: Significant impact of the Magnetic parameter on temperature.

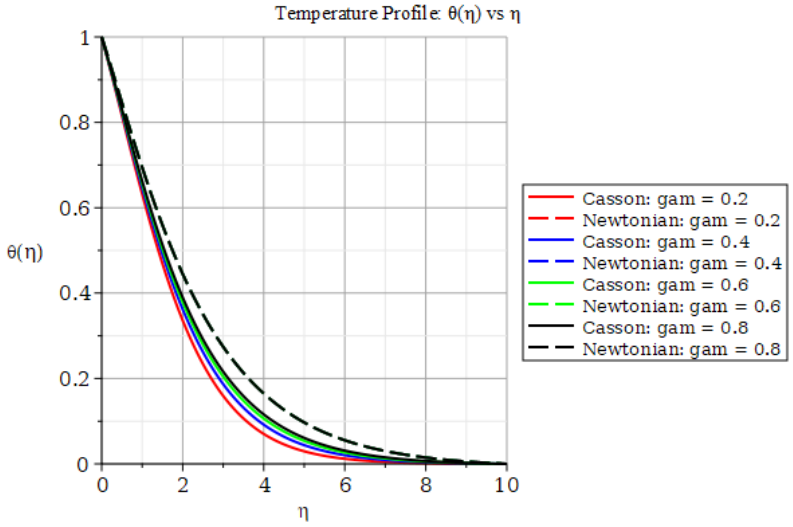

Figure 19: Significant impact of the Casson parameter on the temperature.

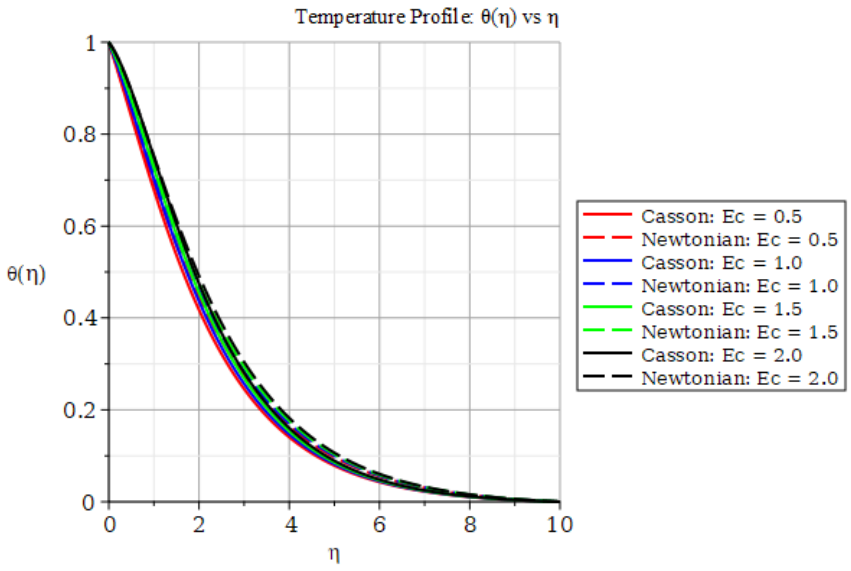

Figure 20: Significant impact of the Eckert number on temperature.

Moreover, the Eckert number Ec, which represents ohmic dissipation, increases the internal heating of the fluid. As Ec rises, ohmic dissipation converts more magnetic energy into thermal energy, raising fluid temperature within the boundary layer. This results in slower thermal decay, a thicker thermal boundary layer, and a smaller wall gradient, thus reducing the Nusselt number and wall heat transfer rate (Fig. **20**). The analysis shows that magnetic field strength and ohmic dissipation reduce heat transfer efficiency, while Casson rheology enhances heat transfer relative to Newtonian fluids. These findings highlight the delicate balance between magnetic suppression, viscous heating, and non-Newtonian effects in controlling thermal transport in MHD Casson fluid systems.

The thermal Grashof number and radiation parameter exert opposite influences on the thermal boundary layer. Increasing Gr strengthens buoyancy forces, which accelerate convective cooling, thin the thermal boundary layer, and enhance the Nusselt number (Fig. **21**). Conversely, increasing N_r intensifies radiative heating, which slows thermal decay, thickens the thermal boundary layer, and reduces the Nusselt number (Fig. **22**). In all cases, Newtonian fluids display stronger cooling and higher heat transfer rates compared to Casson fluids, whose yield-stress properties act to moderate both buoyancy-driven enhancement and radiation-induced suppression of heat transfer.

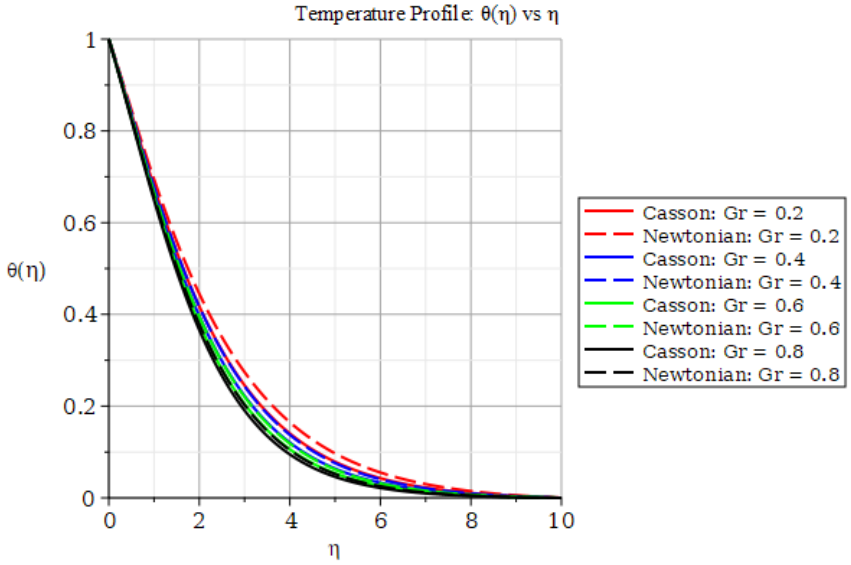

Figure 21: Significant impact of the thermal Grashof number on temperature.

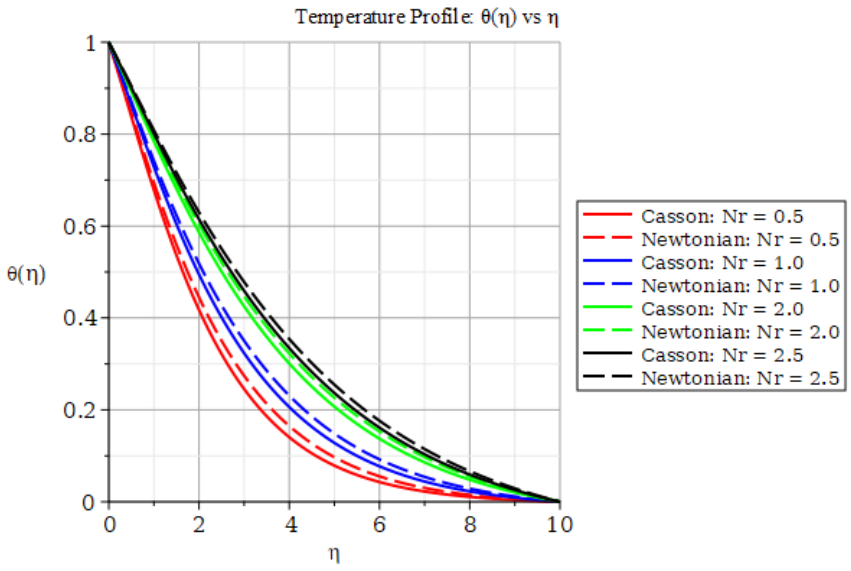

Figure 22: Significant impact of the radiation parameter on temperature.

The Hall parameter m characterizes the influence of Hall currents in a magnetized fluid. As m increases, the electric current is increasingly deflected into the transverse direction, which modifies the Lorentz force distribution and weakens momentum transport in the primary flow direction. This reduction in streamwise convection diminishes heat advection away from the wall, leading to thermal energy accumulation within the boundary layer. Consequently, the temperature profiles increase and the thermal boundary layer becomes thicker, as illustrated in Fig. (**23**).

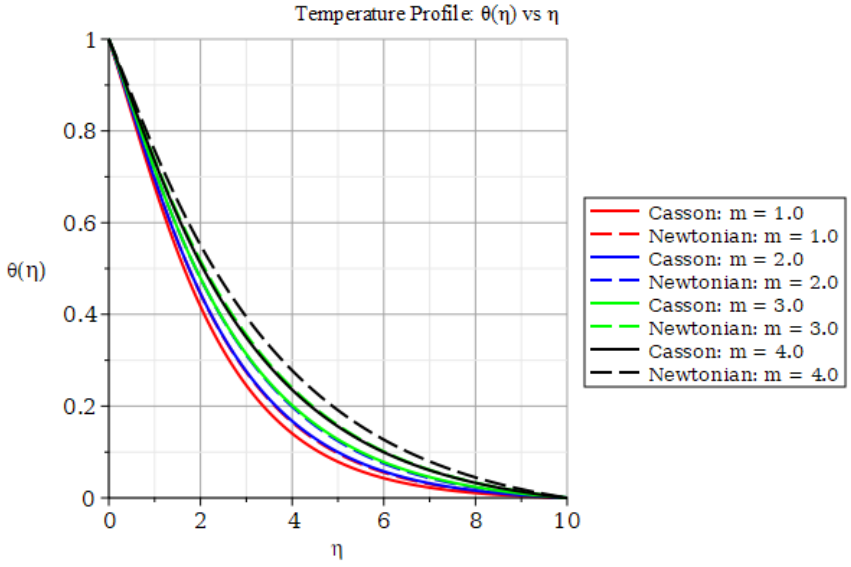

Figure 23: Essential impact of Hall current effect on temperature.

A similar trend is observed with the radiation parameter, which acts as a volumetric heat source and further elevates fluid temperature. When both m and, increase simultaneously, their combined effects significantly suppress convective cooling and enhance thermal diffusion within the boundary layer. This results in a pronounced thickening of the thermal boundary layer and a substantial reduction in the wall temperature gradient, as shown in Fig. (**24**). In all cases, Newtonian fluids exhibit slightly thinner thermal boundary layers and higher heat transfer rates compared to Casson fluids, indicating that yield-stress effects moderate both Hall-induced and radiative thermal transport.

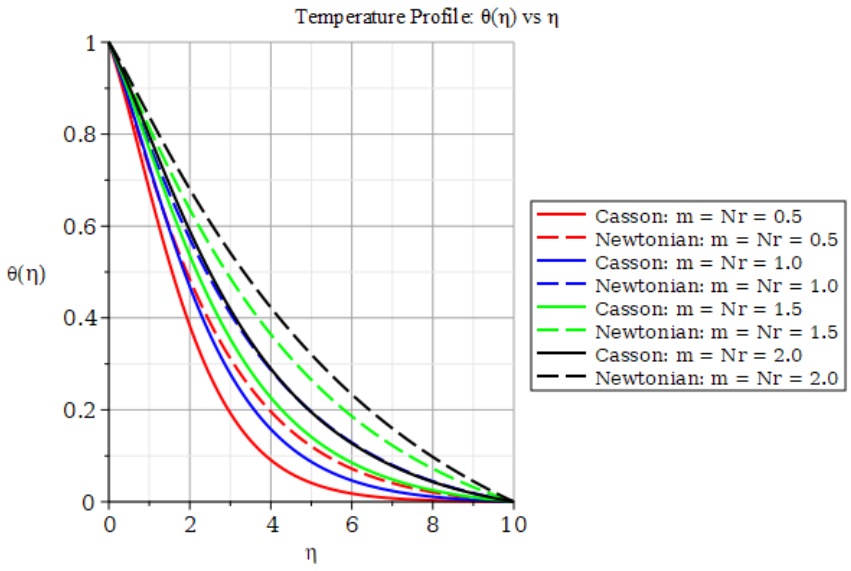

Figure 24: Significant impact of Hall current effect and radiation parameter on temperature.

Fig. (**25**) shows an increase in m resulting in strengthened Hall currents, which alter momentum transport and reduce convective mixing. As a result, solute spreads more slowly away from the wall, resulting in weaker wall concentration gradients. The Sherwood number decreases with higher m, meaning lower mass transfer rates. Casson fluids further suppress diffusion, producing thicker concentration layers compared to Newtonian fluids. The Schmidt number compares momentum diffusivity to mass diffusivity. An increase in Sc means lower mass diffusivity, so the solute penetrates less deeply into the fluid.

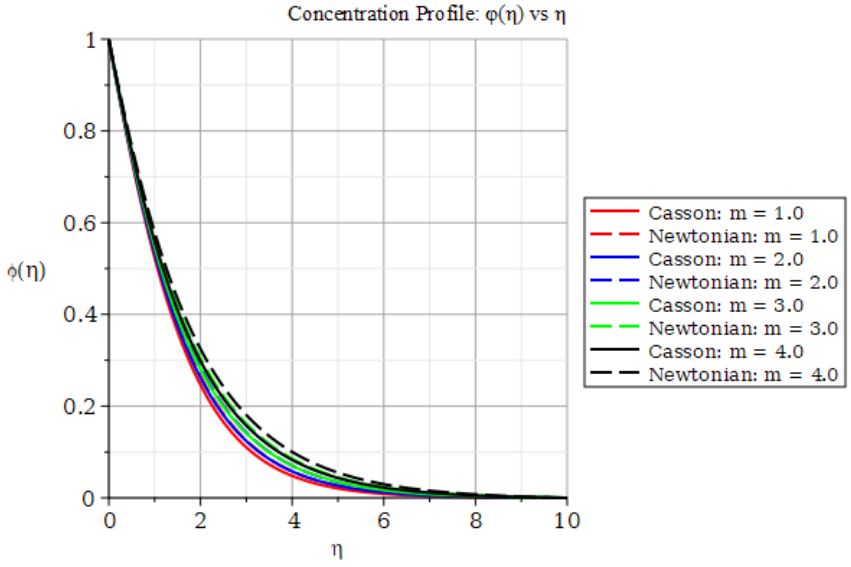

Figure 25: Significant impact of Hall current effect on the concentration.

Fluids with small Sc (like gases with light species) exhibit thick concentration layers, while high Sc fluids (like electrolytes) show thin layers and stronger wall gradients (Fig. **26**). The parameter λ represents the rate of homogeneous chemical reaction. A stronger reaction consumes solute more quickly, reducing its penetration into the boundary layer. This steepens the near-wall concentration gradient, raising the Sherwood number. Therefore, as the reaction rate increases, the mass transfer rate also increases and faster depletion of concentration near the wall. Casson fluids moderate this effect due to their yield stress, giving somewhat thicker concentration layers compared to Newtonian fluids (Fig. **27**).

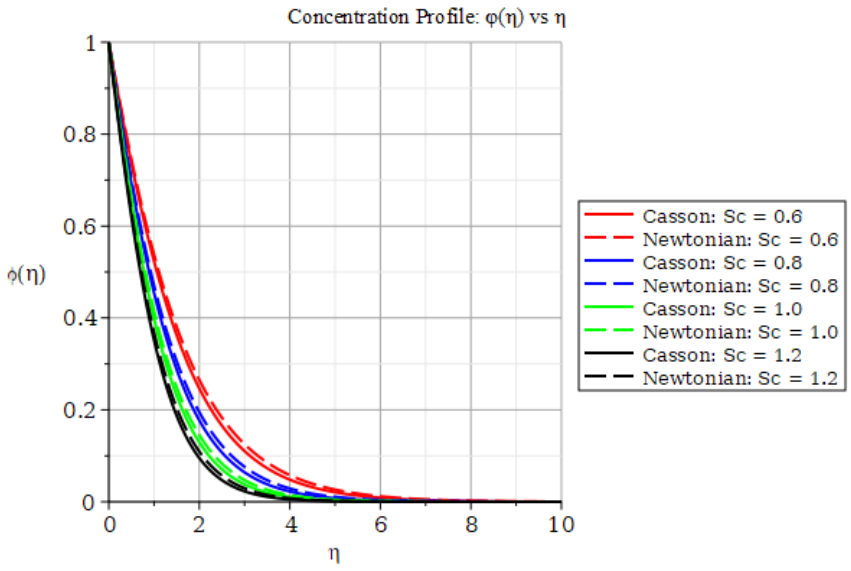

Figure 26: Significant impact of the Schmidt number on concentration.

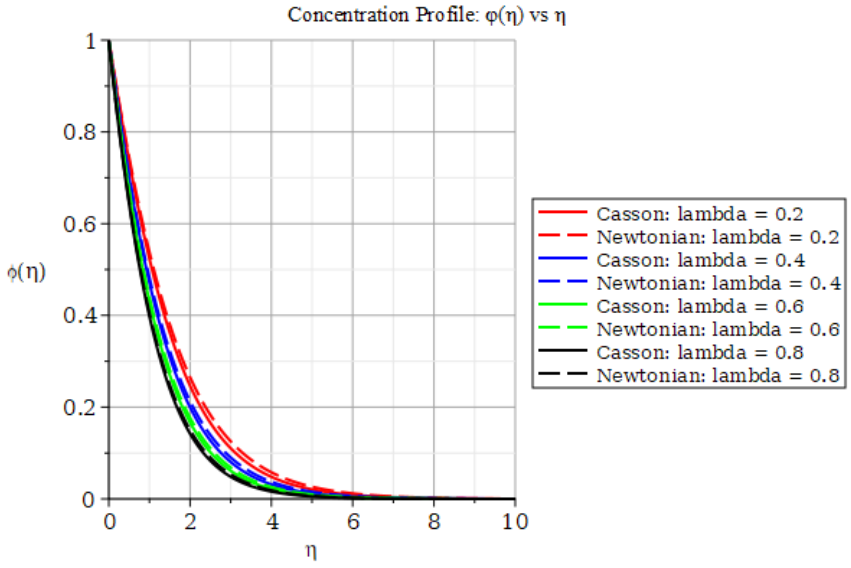

Figure 27: Essential impact of the reaction rate parameter on concentration.

As Gm increases, buoyancy forces due to solutal gradients enhance the upward transport of fluid, which steepens the concentration gradient near the wall. This results in higher Sherwood numbers, indicating that mass transfer is strengthened with increasing solutal buoyancy (Fig. **28**). Fig. (**29**) depicts an increase in the magnetic parameter M produces the opposite effect. The Lorentz force acts as a resistive drag on fluid motion, suppressing convection and weakening the transport of solute away from the wall. Casson fluids consistently exhibit slightly thicker concentration layers and lower Sherwood numbers than Newtonian fluids, demonstrating that yield-stress effects moderate both buoyancy-driven enhancement and magnetically induced suppression of solutal transport. Whereas increasing the Prandtl number (Pr) has the opposite effect, thinning the solutal layer and enhancing Sherwood numbers. Casson fluids always retain solute for longer and exhibit weaker wall gradients compared to Newtonian fluids, highlighting the moderating role of yield stress in solutal transport processes (Fig. **30**).

Casson fluids always retain solute for longer and exhibit weaker wall gradients compared to Newtonian fluids, highlighting the moderating role of yield stress in solutal transport processes. The influence of the Casson parameter (γ) on the concentration profile is illustrated in (Fig. **31**). It is observed that increasing γ increases the thickness of the concentration boundary layer. Physically, larger values of (γ) correspond to reduced yield stress,

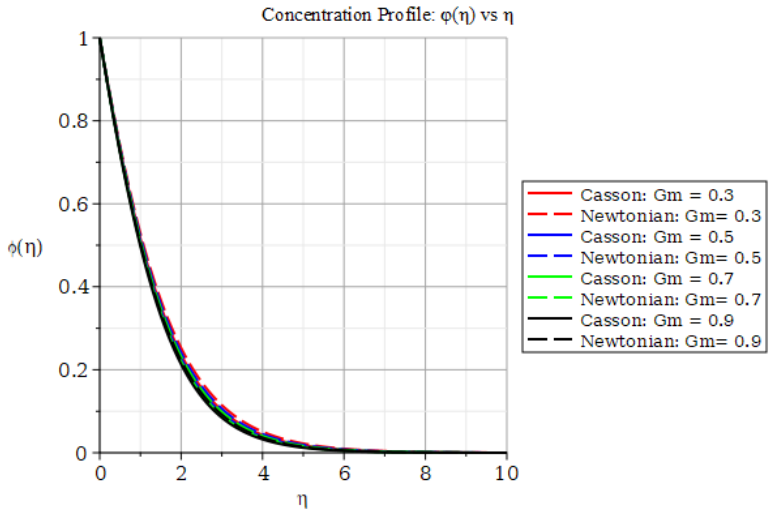

Figure 28: Significant impact of the solutal Grashof number on concentration.

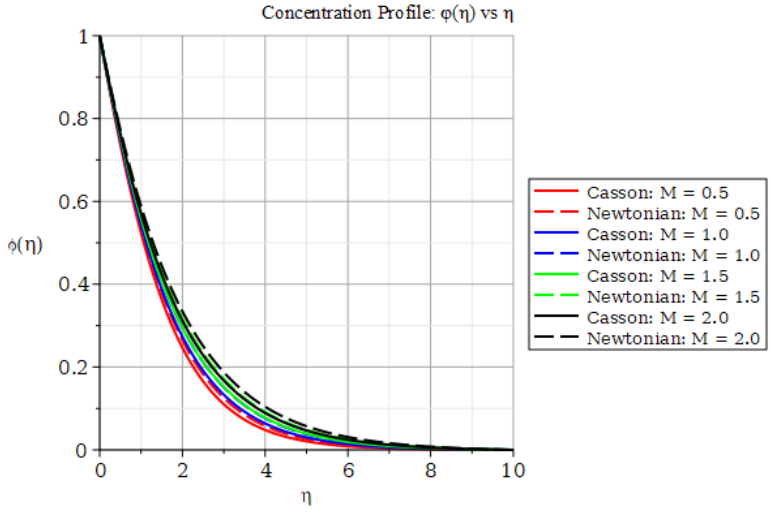

Figure 29: Significant impact of the magnetic parameter on concentration.

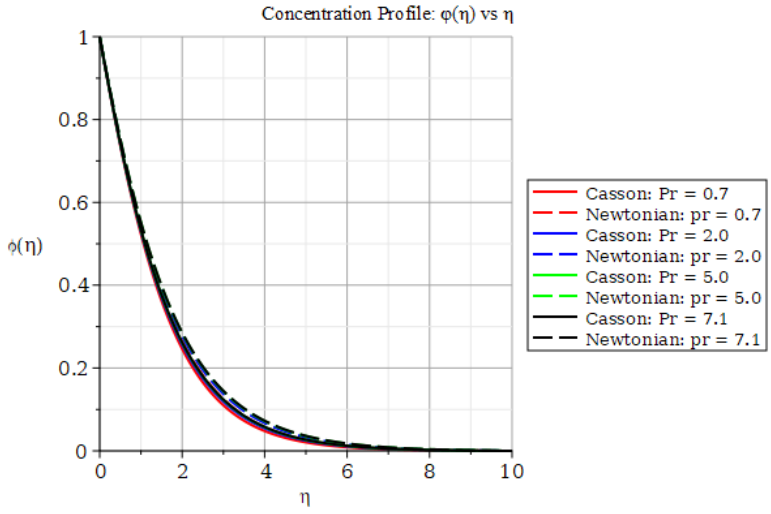

Figure 30: Significant impact of the Prandtl number on concentration.

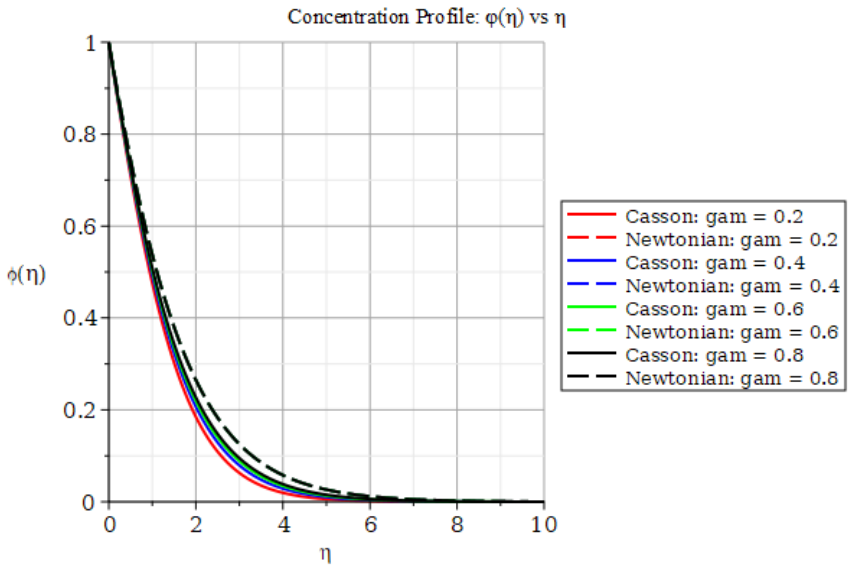

Figure 31: Essential impact of the Casson parameter on concentration.

so the Casson fluid approaches Newtonian behavior and allows more effective diffusion of solute away from the wall. Consequently, the near-wall concentration gradient becomes steeper, which increases the Sherwood number and enhances mass transfer. For lower values of (γ) the fluid exhibits stronger resistance due to higher yield stress, producing thicker solutal layers and lower Sherwood numbers. Casson fluids consistently display thicker concentration layers than their Newtonian counterparts, confirming that non-Newtonian rheology suppresses solutal transport.

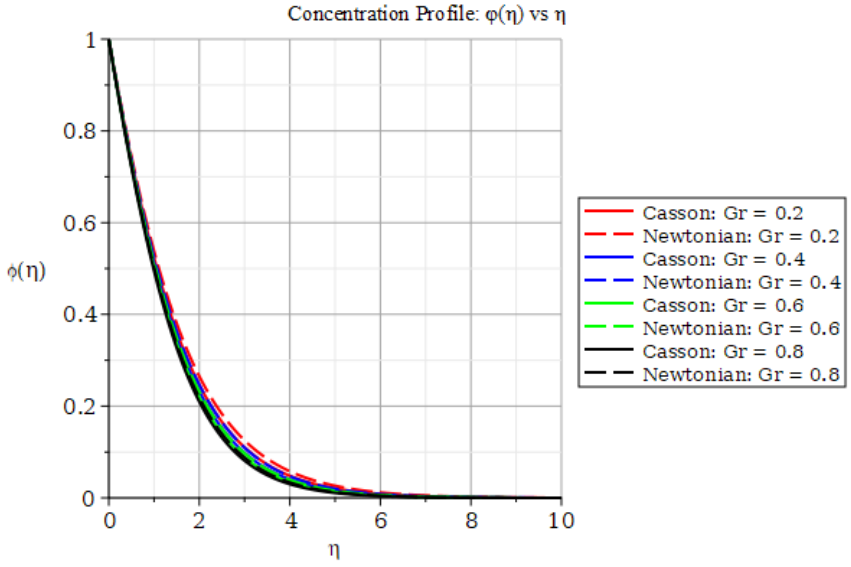

Figure 32: Significant impact of the thermal Grashof number on concentration.

The effect of the thermal Grashof number (Gr) on the concentration field is presented in Fig. (**32**). An increase in Gr enhances buoyancy-driven convection, which thickens the solutal boundary layer. As a result, concentration decays more slowly with distance from the wall. This behavior reflects a reduction in the wall concentration gradient, leading to lower Sherwood numbers and weaker mass transfer rates at the wall. Physically, buoyancy opposes the diffusion of solute away from the wall, retaining higher concentrations near the surface. Casson fluids consistently exhibit thicker solutal layers compared to Newtonian fluids, confirming that non-Newtonian yield-stress effects moderate mass transfer efficiency under thermal buoyancy influences.

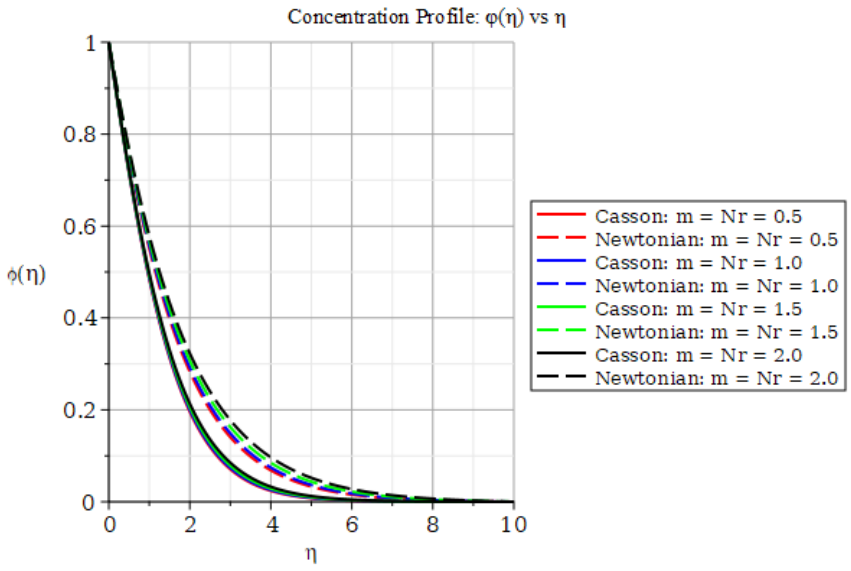

Figure 33: Vital impact of Hall current effect and radiation parameter on concentration.

Fig. (**33**) presents the effect of varying the Hall parameter (m) and the thermal radiation parameter (N_r) on the concentration profile. The results indicate that increasing either m or N_r slows down the decay of concentration, thereby thickening the solutal boundary layer. Physically, higher values of m redistribute the Lorentz force, reducing convective transport of solute away from the wall, while larger N_r enhances radiative absorption, which weakens diffusion processes. In both cases, the near-wall concentration gradient decreases, leading to lower Sherwood numbers and reduced mass transfer rates. Moreover, Casson fluids exhibit consistently thicker solutal layers compared to Newtonian fluids, confirming that yield-stress effects moderate solutal diffusion.

6. Conclusions

In this study, the three-dimensional magnetohydrodynamic Casson fluid flow over a linearly stretching surface is studied under the combined influence of Hall current, thermal radiation, chemical reaction, ohmic dissipation, and buoyancy forces. This is done in response to Hall's current, leading to its own cross-flow velocity component. Numerical solutions for velocity, temperature, and concentration fields were applied to evaluate skin-friction coefficients, Nusselt number, and Sherwood number. The general results are as follows:

- Magnetic parameter (M) and Hall parameter (m) increase both streamwise and cross-flow wall shear stresses but reduce heat transfer rates and mass transfer rates.
- Prandtl number (Pr) promotes heat transfer (Nu) by thinning the thermal boundary layer, but a weak impact on the mass transfer. Casson parameter (γ) thickens velocity and solutal layers with increased scaling, which increases skin friction but decreases Nusselt and Sherwood number while emphasizing yield-stress effect.
- Thermal (Gr) and solutal (Gm) Grashof numbers promote buoyancy, leading to increased heat and mass transfer even at thicker outer layer concentrations.
- The radiation parameter (Nr), in turn, keeps lowering Nusselt numbers over time by heating the boundary layer and the Sherwood numbers by increasing slightly. The chemical reaction parameter (λ) dramatically increases Sherwood numbers as the wall concentration gradients steepen, with only a very small effect on heat transfer.
- The Schmidt number (Sc) confirms its significant impact on mass transport, as it compresses the solutal boundary layer and considerably increases the Sherwood number.

- Eckert number (Ec) influences heat transport non-monotonically. More specifically, at moderate values, Ec decreases Nusselt number due to thermal boundary layer thickening, and at higher values increases heat transfer by increasing near-wall temperature gradients with enhanced dissipation effects.
- Hall current (m) and radiation (Nr) provide synergistic effects that promote enhancement of electromagnetic and radiative heating, which subsequently thickens the thermal and solutal boundary layers, thus reducing heat and mass transfer rates.
- This current analysis has yielded a solid theoretical basis for the study of coupled electromagnetic, thermal and solutal transport phenomena occurring in the Casson MHD flows; it is also a step in the overall progression of non-Newtonian fluid dynamics.

Nomenclature

Roman Symbols

u, v, w	velocity components along x, y, z axes (m/s)
M	Magnetic parameter
m	Hall current
Pr	Prandtl number
Re_x	Local Reynolds number
T	Temperature (K)
T_∞	Ambient Temperature (K)
T_w	Temperature at the wall (K)
$G\mathrm{m}$	Solutal Grashof number
Gr	Thermal Grashof number
C_f	Streamwise skin-friction coefficient
Nu_x	Local Nusselt number
D	Mass diffusivity (m^2/s)
C	Concentration in the fluid (Kg/m^3)
C_∞	Ambient concentration (Kg/m^3)
C_w	Concentration at the wall (Kg/m^3)
q_r	Radiative heat flux (W/m^2)
N_r	Radiation parameter
Ec	Eckert Number
k	Thermal Conductivity (W/m.K)
Sc	Schmidt Number
c_p	Specific heat at constant pressure (J/kg·K)
Sh_x	Local Sherwood number
B_0	Applied magnetic field (T)
C_g	Cross-flow skin-friction coefficient

Greek Symbol

γ	Casson parameter
ρ	Fluid density (kg/m³)
ν	Kinematic viscosity (m²/s)
μ	Dynamic viscosity (Pa·s)
λ	Chemical reaction
α	Thermal diffusivity (m²/s)
σ	Electrical conductivity (s/m)
τ_y	Yield stress of Casson fluid (Pa)
μ_B	Plastic dynamic viscosity of Casson fluid (Pa·s)
π_c	Critical value of product of deformation rates
β_T	Thermal expansion coefficient (1/K)
β_C	Solutal expansion coefficient (1/(kg/m³)
σ^*	Stefan–Boltzmann constant (W/m²·K⁴)
k^*	Mean absorption coefficient (1/m)

Competing Interests

The authors declare that they have no competing interests.

Funding

Not applicable.

Availability of Data

All numerical data generated or analysed during this study are included within the article.

Authors' Contributions

Ibrahim Y. Seini: supervised and made the necessary corrections in the manuscript.

Issah Abubakari: examined and interpreted the findings and was a major contributor in writing the manuscript. All authors read and approved the final manuscript.

References

[1] Khan Z, Rasheed HU, Khan I, Abu-Zinadah H, Aldahlan MA. Mathematical simulation of casson MHD flow through a permeable moving wedge with nonlinear chemical reaction and nonlinear thermal radiation. Materials (Basel). 2022; 15(3): 747. https://doi.org/10.3390/ma15030747

[2] Khan H, Ali F, Khan N, Khan I, Mohamed A. Electromagnetic flow of casson nanofluid over a vertical riga plate with ramped wall conditions. Front Phys. 2022; 10: 1005447. https://doi.org/10.3389/fphy.2022.1005447

[3] Tyfa Z, Reorowicz P, Obidowski D, Jóźwik K. Influence of fluid rheology on blood flow haemodynamics in patient-specific arterial networks of varied complexity-in-silico studies. acta Mech Autom. 2024; 18(1): 8-21. https://doi.org/10.2478/ama-2024-0002

[4] Casson N. Flow equation for pigment-oil suspensions of the printing ink-type. Rheol disperse Syst. 1959; 84-104.

[5] Dhange M, Sankad G, Safdar R, Jamshed W, Eid MR, Bhujakkanavar U, *et al*. A mathematical model of blood flow in a stenosed artery with post-stenotic dilatation and a forced field. PLoS One. 2022; 17(7): e0266727. https://doi.org/10.1371/journal.pone.0266727

[6] Yanala DR, Kumar MA, Bejawada SG, Nisar KS, Raju RS, Rao VS. Exploration of heat and mass transfer on 3-D radiative MHD Casson fluid flow over a stretching permeable sheet with chemical reaction. Case Stud Therm Eng. 2023; 51: 103527. https://doi.org/10.1016/j.csite.2023.103527

[7] Alqahtani H. Impact of newtonian heating on MHD flow of non-newtonian fluid. Int J Mod Phys B. 2025; 39(04): 2540008. https://doi.org/10.1142/S0217979225400089

[8] Seini IY, Aloliga G, Ziblim B, Makinde OD. Boundary layer flow of casson fluid on exponentially stretching porous surface with radiative heat transfer. Diffus Found. 2020; 26: 112-25. https://doi.org/10.4028/www.scientific.net/DF.26.112

[9] Aloliga G, Seini IY, Musah R. On hydromagnetic boundary layer of casson fluid over porous inclined magnetized surface with radiation and convective boundary conditions. Commun Math Appl. 2022; 13(1): 199-221. https://doi.org/10.26713/cma.v13i1.1717

[10] Sulemana M, Seini IY, Makinde OD. Hydrodynamic boundary layer flow of chemically reactive fluid over exponentially stretching vertical surface with transverse magnetic field in unsteady porous medium. J Appl Math. 2022; 2022: 1-11. https://doi.org/10.1155/2022/7568695

[11] Arthur EM, Seini IY, Bortteir LB. Analysis of Casson fluid flow over a vertical porous surface with chemical reaction in the presence of magnetic field. J Appl Math Phys. 2015; 3(6): 713-23. https://doi.org/10.4236/jamp.2015.36085

[12] Dharmaiah G, Goud BS, Srinivasulu T, Sridevi M, Srinu A. Influence of activation energy in steady state hydro dynamic non-Newtonian nano fluid with mobile microorganisms. Results Chem. 2024; 9: 101653. https://doi.org/10.1016/j.rechem.2024.101653

[13] Ali MY, Reza-E-Rabbi S, Ahmmed SF, Nabi MN, Azad AK, Muyeen SM. Hydromagnetic flow of Casson nano-fluid across a stretched sheet in the presence of thermoelectric and radiation. Int J Thermofluids. 2024; 21: 100484. https://doi.org/10.1016/j.ijft.2023.100484

[14] Salem AM, Abd El-Aziz M. Effect of Hall currents and chemical reaction on hydromagnetic flow of a stretching vertical surface with internal heat generation/absorption. Appl Math Model. 2008; 32(7):1236-54. https://doi.org/10.1016/j.apm.2007.03.008

[15] Fatima K, Hymavathi T. Impact of heat source and magnetic field on a thermally radiativehybrid nanofluid flow in a porous medium. Rare Met Mater Eng. 2023; 52(11): 94-102.

[16] Asogwa KK, Ibe AA. A study of MHD Casson fluid flow over a permeable stretching sheet with heat and mass transfer. J Eng Res Reports. 2020; 16(2): 10-25. https://doi.org/10.9734/jerr/2020/v16i217161

[17] Dey D, Borah R. Flow of a Casson fluid with heat transfer over a shrinking sheet and its dual solutions. Songklanakarin J Sci Technol. 2023; 45(1): 80-7.

[18] Saidulu N, Lakshmi AV. MHD flow of Casson fluid with slip effects over an exponentially porous stretching sheet in presence of thermal radiation, viscous dissipation and heat source/sink. Am Res J Math. 2016; 2(1): 1-15.

[19] Alkasasbeh H. Numerical solution of heat transfer flow of casson hybrid nanofluid over vertical stretching sheet with magnetic field effect. CFD Lett. 2022; 14(3): 39-52. https://doi.org/10.37934/cfdl.14.3.3952

[20] Makkar V, Dang K, Sharma N, Yadav S. Numerical investigation of MHD convective free stream nanofluid flow influenced by radiation and chemical reaction over stretching cylinder. Heat Transf. 2023; 52(3): 2328-47. https://doi.org/10.1002/htj.22786

[21] Sawlat N, Qani Y, Sadeqi N. Numerical and symbolic analysis for mathematical problem-solving with maple. J Nat Sci Rev. 2024; 2(3): 29-46. https://doi.org/10.62810/jnsr.v2i3.75

[22] Seini IY. Heat and mass transfer from a convectively heated vertical surface with chemical reaction and internal heat generation. Eng Trans. 2019; 67(1): 101-18.

[23] Talla H. Magnatic field influence on radiative casson fluid flow over an exponetial stretching surface. J Pharm Negat Results. 2022; 13(S6): 1881-88.

[24] Abubakari I, Seini IY. Casson fluid flow through porous media on an exponentially stretched surface in the presence of a transverse magnetic field and chemical reaction. Adv Math Phys. 2025; (1): 5544726. https://doi.org/10.1155/admp/5544726

[25] Leelavathi R, Vyakaranam S, Rao TS, Gurrampati VRR, Oke AS. MHD casson fluid flow in stagnation-point over an inclined porous surface. CFD Lett. 2024; 16(4): 69-84. https://doi.org/10.37934/cfdl.16.4.6984

[26] Yashkun U, Lund LA, Fadhel MA, Shah NA. Velocity slip effect on magnetized casson nanofluid over shrinking/stretching cylinder: duality and stability analysis. Phys Scr. 2024; 99(2): 25203. https://doi.org/10.1088/1402-4896/ad1795

[27] Akaje WT. Stagnation point heat flow and mass transfer in a Casson nanofluid with viscous dissipation and inclined magnetic field. UKH J Sci Eng. 2021; 5(1): 38-49. https://doi.org/10.25079/ukhjse.v5n1y2021.pp38-49

[28] Matveenko VN, Kirsanov EA. Rheology of Structured Liquids. Flow regimes and rheological equations. Colloid J. 2025; 87(1): 38-48. https://doi.org/10.1134/S1061933X24601227

[29] Hazarika GC, Konch J. Effects of Variable viscosity and thermal conductivity on MHD free convective flow along a vertical porous plate with viscous dissipation. Int J Math Trends Technol. 2014; 15: 70-84. https://doi.org/10.14445/22315373/IJMTT-V15P510

[30] Mahabaleshwar US, Mahesh R, Chan A. Stagnation-point brinkman flow of nanofluid on a stretchable plate with thermal radiation. Int J Appl Comput Math. 2024; 10(2): 47. https://doi.org/10.1007/s40819-024-01685-w

[31] Noor NAM, Mahadi S, Nordin NS, Arbin N, Shafie S, Admon MA, *et al*. Squeezing MHD flow of sodium alginate-based casson hybrid nanofluid with soret and dufour effects. J Adv Res Fluid Mech Therm Sci. 2024; 116(1): 97-115. https://doi.org/10.37934/arfmts.116.1.97115

[32] Mahabaleshwar US, Maranna T, Mishra M, Hatami M, Sunden B. Radiation effect on stagnation point flow of Casson nanofluid past a stretching plate/cylinder. Sci Rep. 2024; 14(1): 1387. https://doi.org/10.1038/s41598-024-51963-2

[33] Abbas Khan A, Naveed Khan M, Irfan Shah S, Ashraf M, Matoog RT. Heat and mass transfer exploration of non-Newtonian fluid flow induced by the exponentially stretching Riga surface with the application of Generalized Fourier's and Fick's law. Waves in Random and Complex Media. 2025; 35(1): 1451-66. https://doi.org/10.1080/17455030.2022.2032865

[34] Mehmood R, Khan S, Maraj EN, Ijaz S, Rana S. Heat transport mechanism via ion-slip and Hall current in viscoplastic flow along a porous elastic sheet. Proc Inst Mech Eng Part E J Process Mech Eng. 2022; 236(3): 907-14. https://doi.org/10.1177/09544089211051596

[35] Abbas S, Inam I, Alharthi AM, AL-Khasawneh MAS, Az-Zo'bi EA, Garalleh HAL. Fractional magnetohydrodynamic Casson fluid flow with thermal radiation and buoyancy effects: a constant proportional Caputo model. Bound Value Probl. 2025; 2025(1): 44. https://doi.org/10.1186/s13661-025-02036-4

[36] Mahboobtosi M, Jalili B, Shateri A, Jalili P, Ganji DD. Heat transfer characteristics in the squeezing flow of casson fluid between circular plates: A comprehensive study. Adv Mech Eng. 2024; 16(10): 16878132241290942. https://doi.org/10.1177/16878132241290942

[37] Nandkeolyar R. A numerical treatment of unsteady three-dimensional hydromagnetic flow of a Casson fluid with Hall and radiation effects. Results Phys. 2018; 11: 966-74. https://doi.org/10.1016/j.rinp.2018.10.041

[38] Islam R, Hossain A, Biswas R, Hasan M, Rana BMJ, Habibullah H, *et al*. Modelling and theoretical overview of Casson fluid flow through a stretching sheet with variable viscosity and sinusoidal boundary conditions. Int J Ambient Energy. 2025; 46(1): 2539139. https://doi.org/10.1080/01430750.2025.2539139

[39] Nasir M, Kausar MS, Waqas M, Beg OA, Khan WA. Computational analysis of magnetized Casson liquid stretching flow adjacent to a porous medium with Joule heating, stratification, multiple slip and chemical reaction aspects. Numer Heat Transf Part A Appl. 2025; 86(13): 4464-86. https://doi.org/10.1080/10407782.2024.2319722

[40] Opanuga AA, Adesanya SO, Okagbue HI, Agboola OO. Impact of Hall current on the entropy generation of radiative MHD mixed convection casson fluid. Int J Appl Comput Math. 2020; 6(2): 44. https://doi.org/10.1007/s40819-020-0790-0

[41] Alhadhrami A, Vishalakshi CS, Prasanna BM, Sreenivasa BR, Alzahrani HAH, Gowda RJP, *et al*. Numerical simulation of local thermal non-equilibrium effects on the flow and heat transfer of non-Newtonian Casson fluid in a porous media. Case Stud Therm Eng. 2021; 28: 101483. https://doi.org/10.1016/j.csite.2021.101483

[42] Varatharaj K, Tamizharasi R, Sivaraj R, Vajravelu K, Thameem Basha H. Supervised machine learning analysis of Hall current and radiative effects in Casson nanofluid flow over a stretching surface with activation energy. Int J Ambient Energy. 2025; 46(1): 2549023. https://doi.org/10.1080/01430750.2025.2549023

[43] El-Dabe N, Moatimid GM, Mohamed MAA, Mohamed YM. Effects of Hall currents with heat and mass transfer on the peristaltic transport of a Casson fluid through a porous medium in a vertical circular cylinder. Therm Sci. 2020; 24(2 Part B): 1067-81. https://doi.org/10.2298/TSCI180222185E

[44] Reddy BS, Janaiah C, Raju RS. Double Cattaneo-Christov diffusion effects on radiating three dimensional MHD Nanofluid flow past an exponentially stretching sheet with Multiple Slip effects. J Radiat Res Appl Sci. 2025; 18(3): 101800. https://doi.org/10.1016/j.jrras.2025.101800

[45] Stanciu I, Ouerfelli N. An extended Casson equation for rheological properties of soybean oil at different temperatures and atmospheric pressure. J Biochem Technol. 2020; 11(3-2020): 52-7.

[46] Patel HR. Effects of heat generation, thermal radiation, and hall current on MHD Casson fluid flow past an oscillating plate in porous medium. Multiph Sci Technol. 2019; 31(1): 87-107. https://doi.org/10.1615/MultScienTechn.2019029514

[47] Raptis A. Radiation and free convection flow through a porous medium. Int Commun Heat Mass Transf. 1998; 25(2): 289-95. https://doi.org/10.1016/S0735-1933(98)00016-5

[48] Awwad E, Megahed AM. Enhancing convective heat transfer mechanisms through the rheological analysis of Casson nanofluid flow towards a stagnation point over an electro-magnetized surface. Nanotechnol Rev. 2025; 14(1): 20250220. https://doi.org/10.1515/ntrev-2025-0220

[49] Alrehili M. Nanofluid dissipative stagnation point flow of Casson type over a stretched sheet influenced by a variable surface heat flux and magnetic field. Results Phys. 2024; 58: 107535. https://doi.org/10.1016/j.rinp.2024.107535

[50] Khan MF, Hu G, Sulaiman M. Transformer model learning driven analysis of Casson fluid flow influenced by Hall currents and Darcy-Forchheimer effects. Phys Fluids. 2025; 37(6): 063114. https://doi.org/10.1063/5.0265963

[51] Mukhopadhyay S, Mondal IC, Chamkha AJ. Casson fluid flow and heat transfer past a symmetric wedge. Heat Transf Res. 2013; 42(8): 665-75. https://doi.org/10.1002/htj.21065